AD_____

Award Number DAMD17-94-J-4381

TITLE: Raid 4D MRI of GAD-DTPA Enhancement for Breast Lesion Characterization

PRINCIPAL INVESTIGATOR: Thomas L. Chenevert, Ph.D.

CONTRACTING ORGANIZATION: University of Michigan
Ann Arbor, Michigan 48109-1274

REPORT DATE: April 1999

TYPE OF REPORT: Final

PREPARED FOR: U.S. Army Medical Research and Materiel Command
Fort Detrick, Maryland 21702-5012

REPORT DOCUMENTATION PAGE

Form Approved
OMB No. 0704-0188

1. AGENCY USE ONLY *(Leave blank)*	2. REPORT DATE	3. REPORT TYPE AND DATES COVERED
	April 1999	Final (1 Oct 94 - 31 Mar 99)

4. TITLE AND SUBTITLE
Raid 4D MRI of GAD-DTPA Enhancement for Breast Lesion Characterization

5. FUNDING NUMBERS
DAMD17-94-J-4381

6. AUTHOR(S)
Thomas L. Chenevert, Ph.D.

7. PERFORMING ORGANIZATION NAME(S) AND ADDRESS(ES)
University of Michigan
Ann Arbor, Michigan 48109-1274

8. PERFORMING ORGANIZATION REPORT NUMBER

9. SPONSORING / MONITORING AGENCY NAME(S) AND ADDRESS(ES)
U.S. Army Medical Research and Materiel Command
Fort Detrick, Maryland 21702-5012

10. SPONSORING / MONITORING AGENCY REPORT NUMBER

11. SUPPLEMENTARY NOTES

12a. DISTRIBUTION / AVAILABILITY STATEMENT
Approved for Public Release; Distribution Unlimited

12b. DISTRIBUTION CODE

13. ABSTRACT *(Maximum 200 words)*

The aims of this project were refinement and implementation of new methods designed to defeat the tradeoff between spatial resolution, temporal resolution and tissue coverage in dynamic gadolinium-enhanced MR mammography. The approach involved specialized software for data acquisition and reconstruction to yield dynamic scans of 32 sections through both breasts acquired at 5-6 second temporal resolution. Additional post-processing reduced motion artifacts for improved quantitation via in numerical fitting of temporal enhancement properties of tissues. Technical objectives related to completion of data acquisition and processing methods were generally successful. This methodology was applied in a prospective 4-year study of 102 women referred for surgical biopsy of a breast abnormality detected by non-MRI means. The hypothesis that malignancies to will display a high contrast-enhancement rate was supported by the data [rate = $(79 \pm 75)\times10^{-3}$ sec^{-1}, mean ± std dev, N=39] relative to benign tissues [rate = $(19 \pm 16)\times10^{-3}$ sec^{-1}, N=54], although some overlap exists. ROC analysis yields a sensitivity 85% and specificity 75% using an enhancement-rate threshold = 22×10^{-3} sec^{-1}. These quantitative kinetic properties can be further combined with tissue/lesion morphology to further enhance specificity of breast MRI.

14. SUBJECT TERMS
Breast Neoplasm Diagnosis, Fast Magnetic Resonance Imaging, Enhancement time-Course Analysis, Clinical Imaging

15. NUMBER OF PAGES 29

16. PRICE CODE

17. SECURITY CLASSIFICATION OF REPORT	18. SECURITY CLASSIFICATION OF THIS PAGE	19. SECURITY CLASSIFICATION OF ABSTRACT	20. LIMITATION OF ABSTRACT
Unclassified	Unclassified	Unclassified	Unlimited

FOREWORD

Opinions, interpretations, conclusions and recommendations are those of the author and are not necessarily endorsed by the U.S. Army.

NA Where copyrighted material is quoted, permission has been obtained to use such material.

NA Where material from documents designated for limited distribution is quoted, permission has been obtained to use the material.

✓ Citations of commercial organizations and trade names in this report do not constitute an official Department of Army endorsement or approval of the products or services of these organizations.

NA In conducting research using animals, the investigator(s) adhered to the "Guide for the Care and Use of Laboratory Animals," prepared by the Committee on Care and use of Laboratory Animals of the Institute of Laboratory Resources, national Research Council (NIH Publication No. 86-23, Revised 1985).

✓ For the protection of human subjects, the investigator(s) adhered to policies of applicable Federal Law 45 CFR 46.

NA In conducting research utilizing recombinant DNA technology, the investigator(s) adhered to current guidelines promulgated by the National Institutes of Health.

NA In the conduct of research utilizing recombinant DNA, the investigator(s) adhered to the NIH Guidelines for Research Involving Recombinant DNA Molecules.

NA In the conduct of research involving hazardous organisms, the investigator(s) adhered to the CDC-NIH Guide for Biosafety in Microbiological and Biomedical Laboratories.

✓ 5/4/99

PI - Signature Date

TABLE OF CONTENTS **Page**

INTRODUCTION

Gadolinium-based magnetic resonance (MR) contrast agents offers exceptionally high sensitivity for the detection of breast cancers [1-6]. The specificity of gadolinium-enhanced MR mammography to distinguish benign from malignant tissues, however, has been limited by the fact that some normal and benign masses also exhibit substantial contrast enhancement [3,5,6]. Alternatively, properties related to the "temporal rate" of contrast uptake has being studied as a potential complimentary discriminator of benign from malignant breast neoplasm [7-11]. Investigators have noted, malignancies tend to exhibit a rapid contrast enhancement profile that is presumably due to an anomalous vascular supply and highly permeable capillaries. Non-invasive methods to detect and/or discriminate between normal, benign, pre-malignant and malignant tissues based on vascular alterations would have significant diagnostic value, particularly in cases that are a challenge for conventional mammography such as in dense breasts.

Acquisition and processing methods to quantify MRI contrast agent enhancement kinetics have been widely variable across studies [7-11]. For accurate characterization of contrast uptake features of breast lesions in a clinical setting, critical parameters include: temporal resolution, spatial resolution, volume of tissue coverage, and the method to quantify signal changes. Information regarding "rate of enhancement" is obscured if the temporal sampling is inadequate to record details of the lesion enhancement curve such as the point contrast onset and maximal slope. More serious errors occur if the imaged volume only partially includes an enhancing lesion or does not include all lesions in the breast. These issues arise, in part, due to the well known trade off between volume coverage, spatial resolution, and temporal resolution.

The central objectives of this project are technical refinement and clinical implementation of new dynamic contrast-enhanced MRI methods designed to provide full volume coverage of both breasts at good spatial and temporal resolution for detailed quantification of dynamic contrast enhancement properties [10]. Key elements of this approach involved specialized software for data acquisition (i.e. MRI pulse sequence), motion correction and image reconstruction, and kinetic analysis of contrast-enhanced tissues. The methodology developed for this project allowed dynamic scans through 32 sections of both breasts acquired at 10-13 second temporal resolution - this was a 4 fold higher temporal sampling than the commercially available sequence. Additional post-processing, referred to as viewsharing, further reduced temporal sampling to 5-6seconds. This technique was applied to study 102 women in whom a breast abnormality was detected by mammography, physical exam, or ultrasound.

METHODS

MRI Data Acquisition

Breast MR exams were performed on 1.5Tesla General Electric Signa systems using a commercial (GE) bilateral phased-array breast coil with insert pads for mild anterio/posterior (A/P) compression. The MRI protocol for all patients was as follows:

Series 1: Axial Locator

Axial sections 10mm thick; 2D Spin-Echo (SE); Echo-Time (TE)=12ms; Rep-Time (TR)=300ms; Matrix = 256x128; Field-of-View (FOV)=35cm; Excitations (NEX)=1; ScanTime = 1min 29sec.

Series 2: Axial T2-weighted

Axial sections 6mm thick; 2D Fast-Spin-Echo (FSE, 8echo-train); TE=102ms; TR=3000ms; Matrix = 256x192; FOV=28-32cm; NEX=2; Fat signal suppressed (FatSat); Freq axis=Ant/Post; ScanTime = 5min 23sec.

Series 3: Axial T1-weighted Pre-Contrast

Axial sections 6mm thick; 2D; Phase-Offset-Multi-Planar; TE=14ms; TR=400ms; Matrix = 256x192; FOV=28-32cm; NEX=2; Fat signal suppressed (FatSat); Freq axis=Ant/Post; ScanTime = 5min 20sec.

Series 4A: Coronal 3D T1-weighted Pre-Contrast

Coronal sections 2-5mm thick; 32slices; 3D Spoiled Gradient-Recalled Echo (SPGR); TE=3.3ms; TR=10ms; Flip=40°; Matrix = 256x128; FOV=28-32cm Rt/Lt, FOV=14-16cm Sup/Inf; NEX=4; ;Freq axis=Rt/Lt; ScanTime = 2min 38sec.

Series 4B: Dynamic Coronal 3D T1-weighted

Repeat 4A with Matrix = 256x32 and NEX=1 in each pass; 20 passes, then one pass of Matrix = 256x128; Scan Time = 4min 6sec.

Series 4C: Coronal 3D T1-weighted Post-Contrast

Repeat 4A Scan Time = 2min 38sec.

Series 5: Axial T1-weighted Post-Contrast

Repeat Series 3; ScanTime = 5min 20sec.

The dynamic series was built upon a 3D-volumetric rf-spoiled gradient recalled echo (3D SPGR) sequence since it (a) offers excellent sensitivity to gadolinium-induced changes, (b) produces high signal-to-noise images, and (c) provides full volume coverage of both breasts with contiguous image sections. Series 4 segments A, B, and C were concatenated for speed and to eliminate need for machine adjustment; this helped minimized patient movement. A standard dose of gadolinium-contrast material (0.1mMol/kg; Magnevist, Berlex Labs, Wayne, NJ.) was manually injected as a bolus at a specified time during segment B.

MRI Data Processing

Scan time and spatial resolution are proportional to acquisition matrix size. Dynamic changes (due to gadolinium), however, are most heavily concentrated near the center of the 3D Fourier-encoded MRI dataset referred to as "k-space". Therefore, to successfully record most dynamic contrast changes, while greatly reducing scan times for high temporal resolution (i.e. a 3D image set every 10 seconds), only the central k-space data

were acquired during the gadolinium injection (i.e. Series 4 B). The lost spatial resolution was partially restored by reuse of previously acquired peripheral k-space data (i.e. from Series 4 A). This process of splicing high temporal resolution central k-space data blocks with high spatial resolution peripheral k-space data is referred to as the "keyhole" method, and was extended to 3D specifically for this study [10].

An additional a post-processing technique referred to as "viewsharing", was applied to effectively double the temporal sampling rate to a 3D image set every 5 seconds. Viewsharing is the synthesis of data blocks at each intermediate timepoint by combination of the latter half of a given data keyhole block with the initial half of the subsequent data block. As with each original keyhole data block, synthetic viewshared blocks were submitted for keyhole reconstruction. In this study, a series of 21 keyhole blocks were acquired and interleaved with 21 viewshared blocks for a total 42-point timeseries spanning 4-5minutes.

Contrast enhancement analysis requires that the patient remain relatively still during all of Series 4; often this was not the case. A simple linear motion correction algorithm was incorporated within keyhole/viewshared image reconstruction to reduce motion artifacts. The algorithm is described in detail elsewhere (Medical Physics, in press; see appendix), but briefly it involves matching the phase of each k-space block to the pre-contrast k-space data. In effect, this phase adjustment is equivalent to a 3-dimensional translation of each imageset toward spatial coregistraion with pre-contrast images. Since the pre-contrast data also serves as a subtraction mask, this correction reduced motion artifacts that are most apparent on subtracted images. Motion-corrected, viewshared, keyhole anatomic and subtracted images were viewed cinegraphically on the SUN SPARC10 workstation where all reconstruction/analysis was performed. Rapidly enhancing lesions are most conspicuous on the cinegraphic subtracted images. This CINE format aided the user to electronically define a region of interest (ROI).

Lesion ROI enhancement vs time curves were automatically fit to exponential saturation, and exponential saturation-decay models. These mathematical functions are derived from compartmental models that describe the temporal distribution of contrast media between tissue vascular and extracellular spaces. These models, albeit simplistic, suggest that capillary permeability and surface area (P•S product) are most relevant to early enhancement rate. Enhancement rate is defined as [fitted enhancement time, tau]$^{-1}$. Also, overall enhancement amplitude (i.e. degree of signal change) reflects size of extracellular space and amount of contrast leakage. Fitted enhancement amplitude and temporal properties were recorded on disk for each ROI. Image excerpts, contrast enhancement curve, and fitted results for an invasive carcinoma are illustrated in Figure 1.

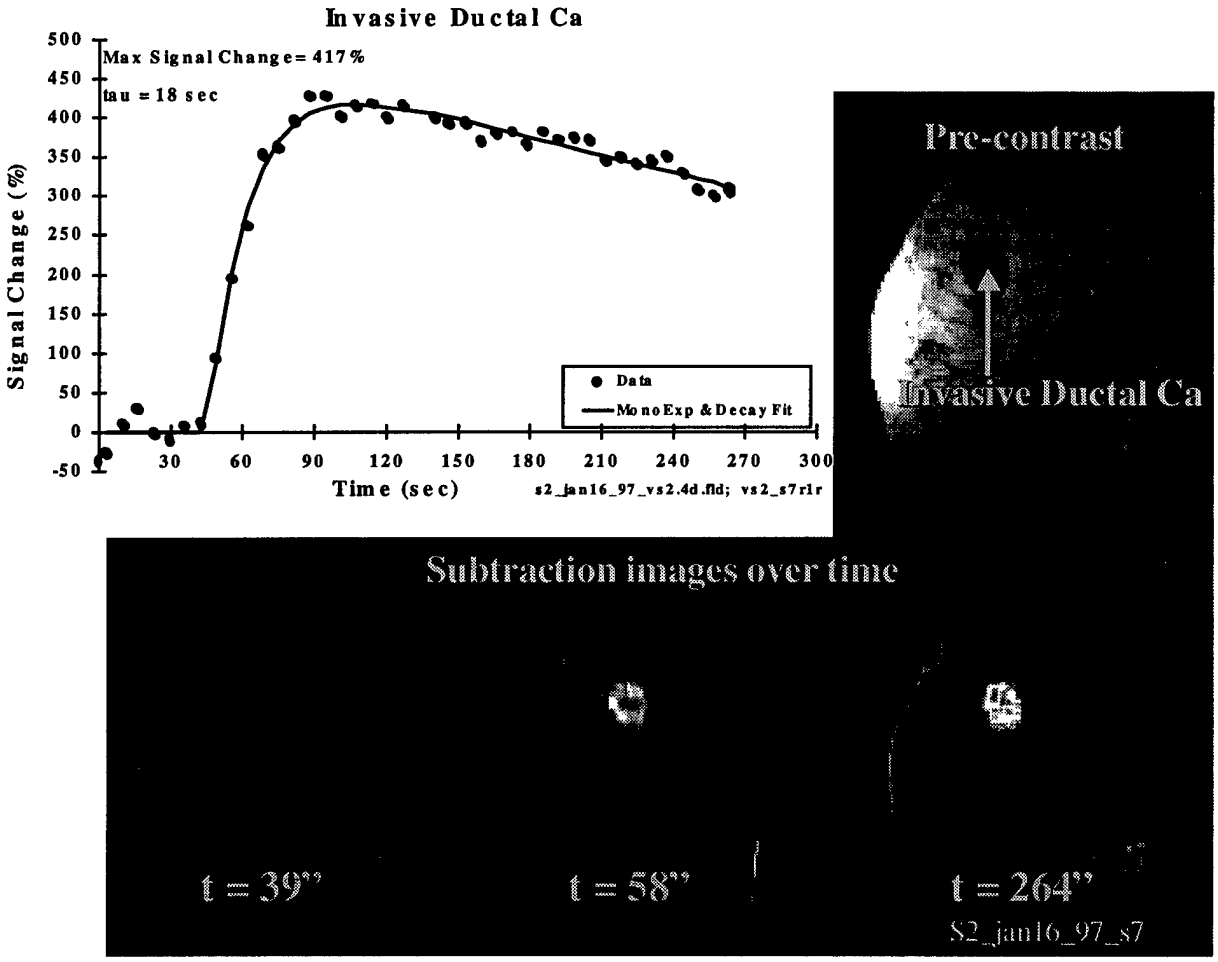

Figure 1. Excerpts from an enhancement time series of a invasive ductal carcinoma in the upper-outer quadrant of the right breast. This lesion exhibits a high enhancement rate ($P \bullet S \sim 1/18sec = 57x10^{-3}sec^{-1}$) and washout; both signs are strongly suggestive of cancer.

Patient Recruitment - Image Review

Recruited patients were referred from the Breast Care Center of the University of Michigan Comprehensive Cancer Center. Entrance criteria includes any patient with a breast abnormality detected by mammography, physical examination, or ultrasound, and which will be biopsied. Prior to MRI study, all patients had a routine clinical evaluation which included mammography/ultrasound and breast physical examination.

Images/films/reports were reviewed by radiologists (project co-Investigators) in the order of: (a) conventional mammography images (Xray, ultrasound) and previous reports; (b) conventional MRI including pre- and post-gadolinium; and (c) subtracted MR images (pre-gad subtracted from post-gad). The radiologist defined which slice/region best corresponded to the lesion/tissue sampled by surgical/core biopsy. Occasionally, additional focal tissues were noted on MRI that were correlated with mammographically-stable (>1year) lesions. These were also included in the analysis as benign lesions.

Statement of Work Tasks and Status

SOW Task 1: Patient recruitment - uniform over the four years of the study
One-hundred breast patients will be studied during this four-year prospective imaging trial. Volunteer patients will be recruited from the Breast Imaging Section of the Breast Care Center at the University of Michigan Hospital. Entrance criteria will include patients with a breast abnormality detected by mammography, physical exam, or ultrasound which will be biopsied. Malignancy, grade, type and lymph node involvement will be determined for each patient by pathologic reading. Approximately 30 malignant and 70 benign lesions are expected from this population.

Status Task 1: Originally, one-hundred women were to be recruited for this study. Ninety-four women were enrolled and scanned during project period; two failed to complete the MRI exam due to claustrophobia. An additional ten women were included from the pilot study completed prior to the project period. The same scan/processing techniques applied and these women had biopsies. This provided data from a total of 102 subjects. Per the stated selection criteria, any patient with an abnormality sufficient to warrant biopsy was considered for this study. This was done to not limit selection to only those with highly suspicious discrete masses. As such, a relatively large number of patients were included in the study by being referred for architectural distortion and/or calcification clusters, but without having a discrete mass. In some of these cases focal enhancement in the region of mammographic concern made correlation of biopsy sampling and MRI ROI definition straightforward. In cases lacking focal enhancement in the region of mammographic abnormality the correlation of the biopsy/surgical site on the MRI was more difficult. In 27 cases, the radiologist used the mammogram and MR images to provided a "best estimate" of the biopsy area on the MRI even though the MRI exhibited non-focal or moderate parenchymal enhancement. All of these 27 cases would have been read as "negative" by MRI due to lack of focal enhancement. The pathology results on these 27 cases were all non-malignant - most common path reading was fibrocystic change, with or without calcifications. In the interest of testing the value of the quantitative MRI parameters, data from these ROI's were maintained in the statistical analysis described in the Results. At the project end, quantitative enhancement data were collected from total of 39 cancer and 54 non-cancer tissues.

SOW Task 2: Enhancement rate-constant determination - each patient
Each patient will be studied by a new dynamic MRI sequence during bolus administration of gadolinium-DTPA contrast. The data acquisition and processing sequence will generate a temporal series of 32 data sets, where each set represents 32 tomographic slices through both breasts, acquired at a rate of 1 set per 10-13 seconds. Existing specialized interactive software will be employed to retrospectively view each tomographic slice cinegraphically to identify gadolinium enhanced tissues. Enhancement rate-constants will be quantified by numerical fit to signal change versus time using a exponential saturation model.

Status Task 2: Complete.

SOW Task 3: Software development: View Sharing & Automated Fitting - 1st year
View sharing is a post-processing concept designed to effectively double the dynamic sampling rate using existing data. Software to execute and test this concept will be written for simulated and actual MRI data. Pending satisfactory performance of view sharing, archived data sets will be reprocessed, and subsequent data sets will be processed with view sharing thus yielding 64 data sets at 6sec dynamic temporal resolution. Addition development work will be directed toward export of datasets from workstation back into MRI system database for more portable viewing.

Status Task 3: Complete. Keyhole reconstruction, viewsharing, and motion-correction algorithms were applied to each case. Total number of viewshared datasets, however, was limited by computer memory to 42 timepoints instead of 64. We do not believe this change affected results since the critical "rapid-enhancement" segment of the curve happens early in the timeseries. We elected to retain dynamic breast image datasets on the workstation since transferal and storage of large image sets (>2000 images per case) is cumbersome. Instead, we added a high-quality hardcopy unit and a 2.6Gbyte magneto-optical drive to the SPARC10 workstation, thus harcopy/analysis on the MRI system was not essential.

SOW Task 4: Statistical summary - final two months of study
Quality of curve fitting and appropriateness of selected model will be statistically assessed on individual patient data. This will be performed throughout the study, as will assembly of other diagnoses and pathological outcomes into a database. Final inter-patient statistical summaries will occur in the last few months of the study. Quantitative enhancement rate constants, conventional pre-biopsy diagnosis, and pathologic characterization will be submitted for statistical testing of stated hypotheses regarding diagnostic sensitivity, specificity, positive and negative predictive values of enhancement rate constants relative to conventional pre-biopsy diagnosis. Classification power for tissue group type, and correlation with tumor grade, size, invasiveness, and lymph node involvement will be determined.

Status Task 4: Near Complete. Statistical analyses are complete for MRI parameter fits to: (a) enhancement time, τ, (time-constant of the exponential enhancement curve); (b) enhancement rate ($1/\tau$) related to permeability surface-area product; (c) enhancement amplitude; and (d) product of enhancement rate and amplitude for available ROIs. Since these are objective numerical classifications of cancer vs non-cancer, a Receiver Operating Characteristic curve was developed for each MRI parameter. Note, these MRI parameters are based on enhancement kinetics and are independent of visual "morphology" cues used by the radiologist. Certainly, morphologic signs of smooth/rounded versus irregular/spiculated lesion borders are diagnostically important properties. Morphology-based reading of the MRI relative to mammography and the analysis, is more time consuming. This aspect of the study is ongoing using the existing

patient database. When completed, results of the clinical reading study will be summarized in a subsequent publication.

RESULTS

Spatial correlation between pathology, radiologic follow-up (>1years) and ROIs quantified by MRI was achieved for 93 lesions/tissues with the quantitative results summarized in the Table below.

Table

Mean ± StdDev of MRI-derived Contrast Enhancement Kinetic Properties

Tissue Type	Enhancement Time Constant [sec]	Enhancement Rate (~ P•S) [10^{-3} sec^{-1}]	Enhancement Amplitude [% Signal Change]	Enhancement Amplitude x Enhancement Rate
Benign (N=54)	135 ± 364	19 ± 16	132 ± 139	4 ± 11
Malignant (N=39)	27 ± 40	79 ± 75	211 ± 101	18 ± 21
p value	0.052	< 0.001	0.03	< 0.001

Of the quantitative MRI parameters studies, enhancement rate provided the greatest discrimination between benign and malignant tissues in our database. Figure 2 illustrates

Figure 2

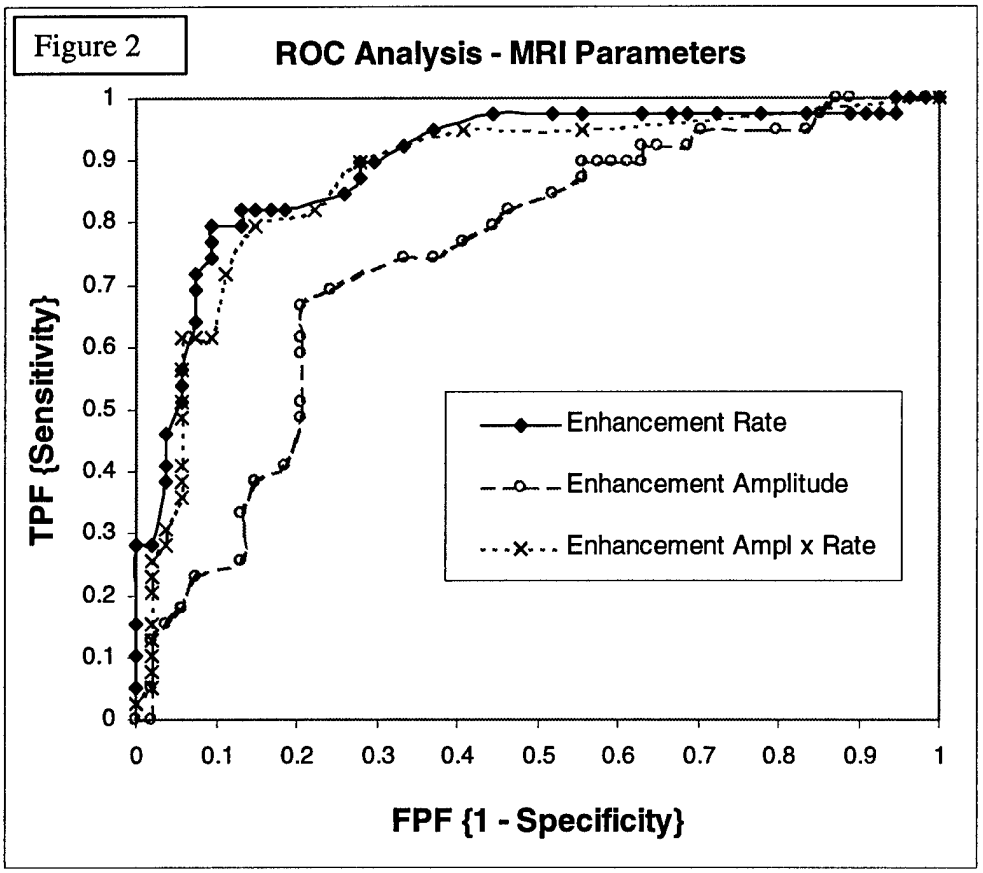

ROC curves for Enhancement Rate, Amplitude and Rate x Amplitude. Good quality Xray mammography targets a Sensitivity >85% and Specificity >90%, and a positive predictive value (PPV) of 25%-40% for women recommended to biopsy [12]. The MRI ROC on quantitative (non-morphologic) data suggests a Sensitivity ≈85% and Specificity

≈75%. The enhancement rate decision threshold at this Sensitivity/Specificity point was Enhancement Rate = 22/sec = 1000/Tau, which corresponds to an enhancement time constant of 43seconds. The MRI PPV was 72% at this decision threshold. The aggregate of individual tissue/lesion enhancement data are shown in Figure 3.

Figure 3: Scatterplots of enhancement properties as a function of tissue type. Note, Tissue Types 1 - 5 are considered benign and Tissue Types 6 - 11 are malignant. (A) enhancement time constant; (B) enhancement amplitude; (C) enhancement rate, which is primarily dependent on PS product and (D) enhancement amplitude x rate.

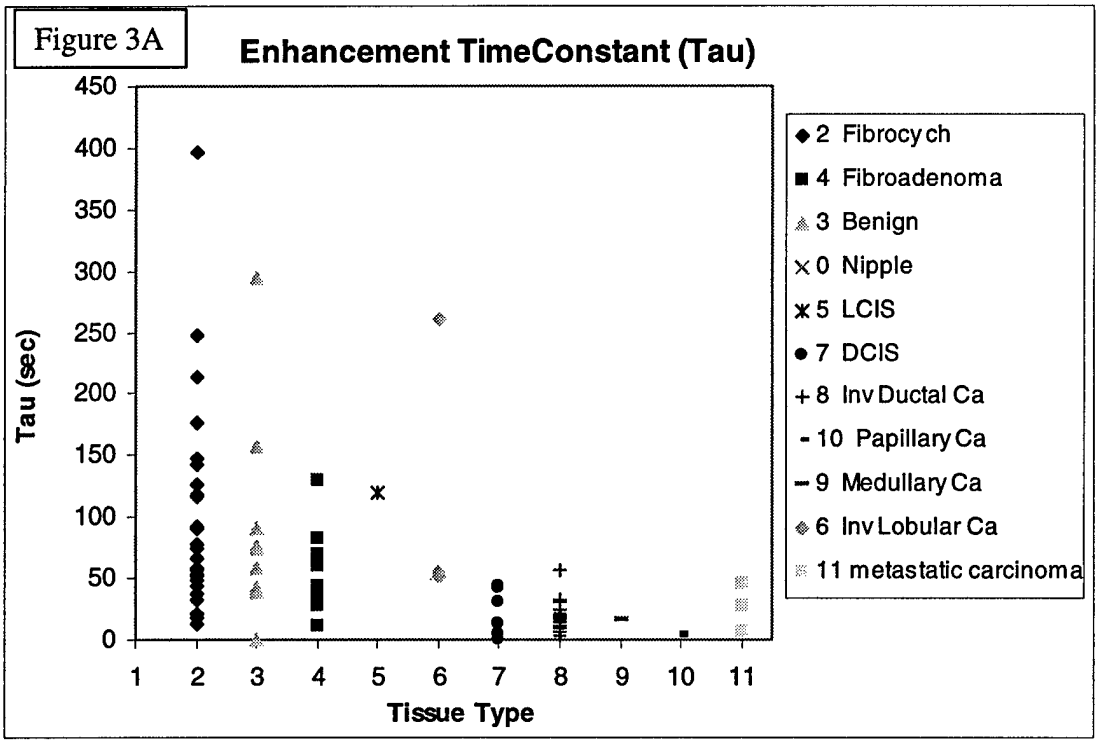

Figure 3B

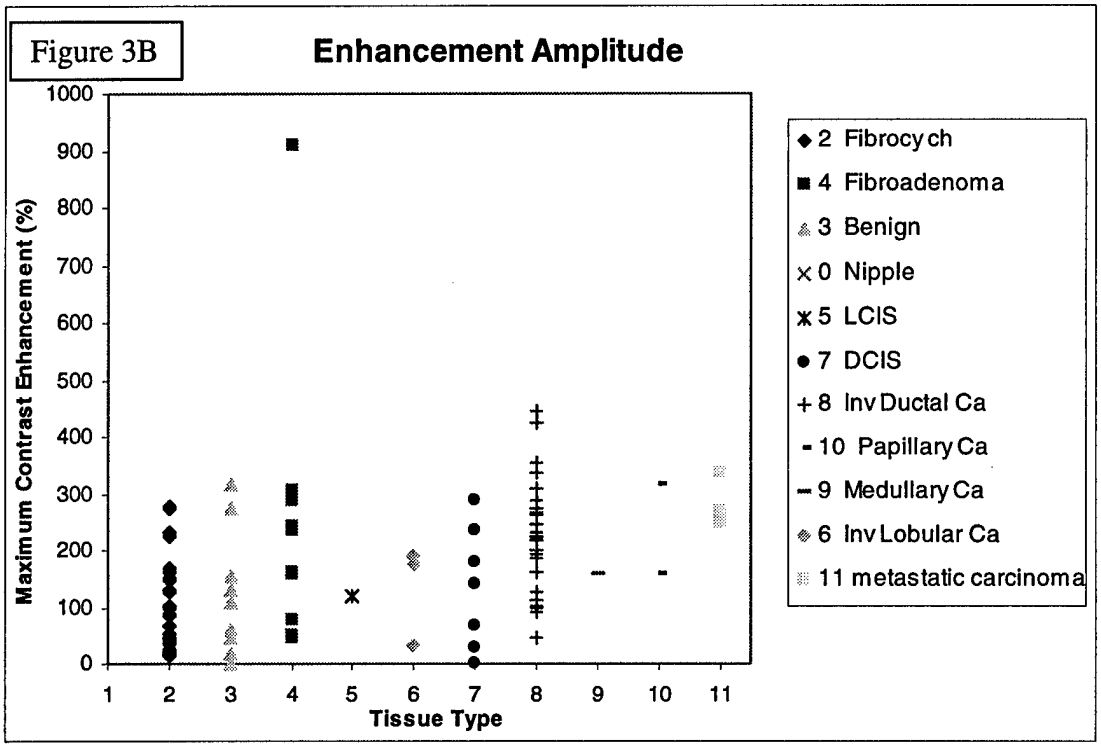

Figure 3C

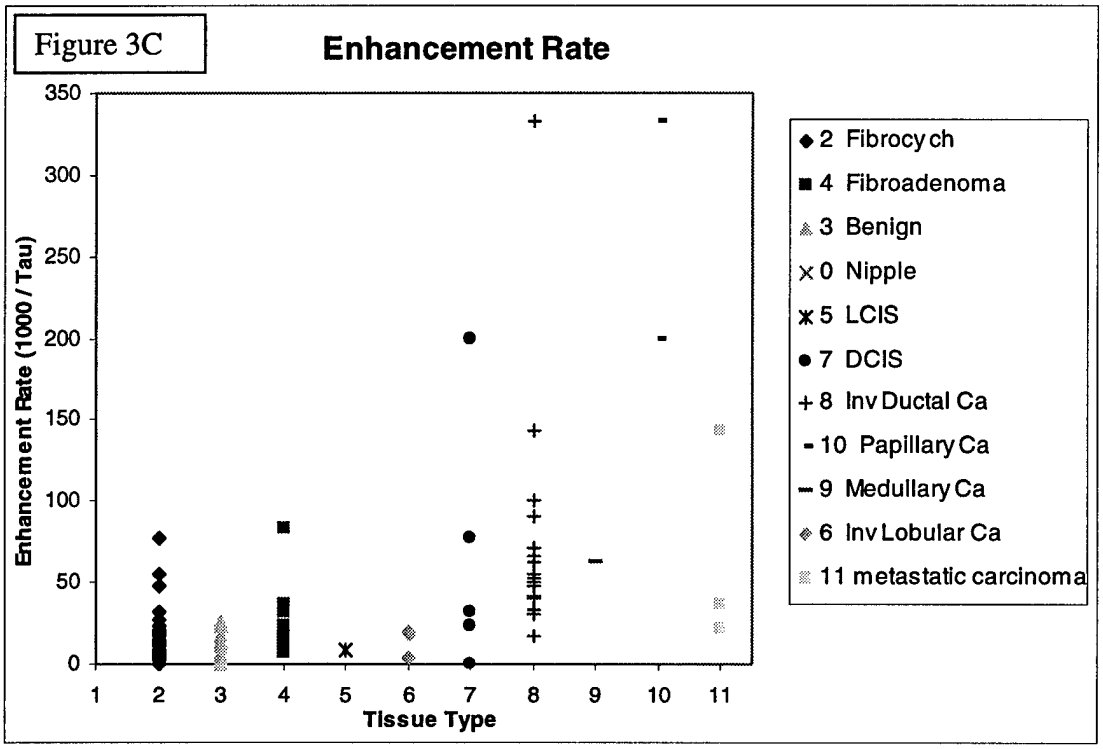

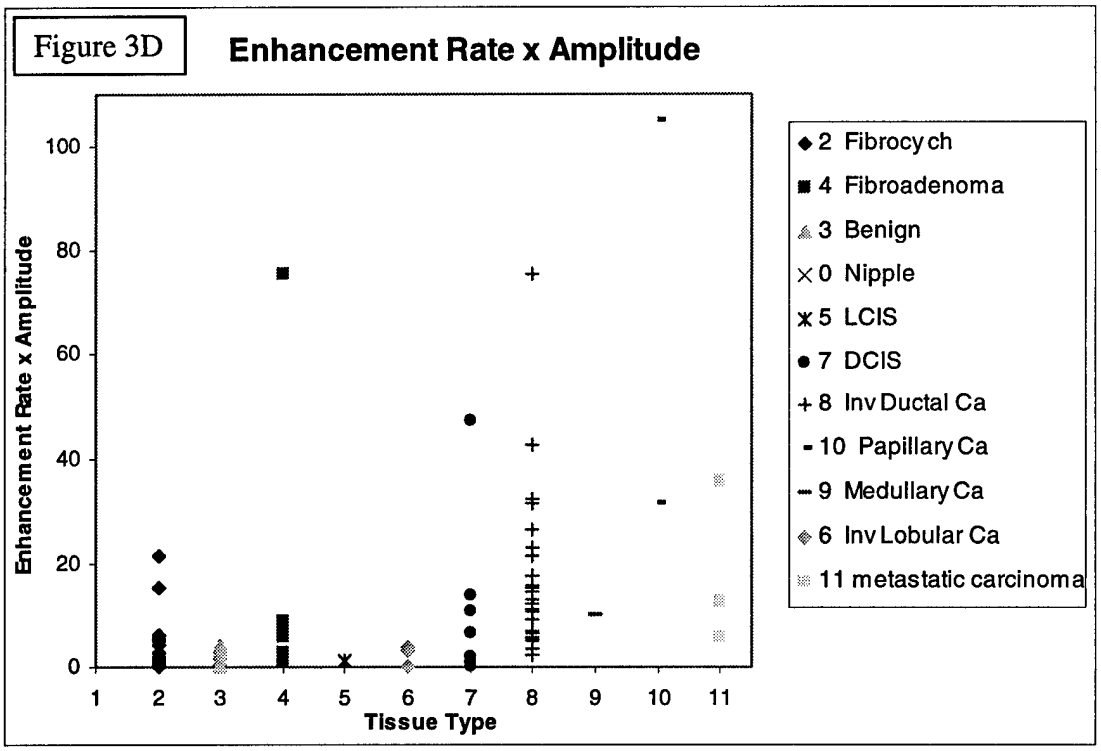

CONCLUSIONS

Technical objectives of high temporal sampling and good spatial resolution for quantitative description of breast lesion enhancement properties were satisfied by the methodology developed for this study. Viewsharing increased temporal resolution to 5-6second sampling, however, a comparison of fitted kinetic parameters on viewshared data versus without viewsharing (i.e. 10-12second temporal sampling) suggest there is not a quantitative advantage to viewsharing. There is, however, a minor cosmetic improvement on cinegraphic images. Given this, we believe temporal sampling below 10sec imageset is not required for kinetic characterization of breast tissues. Moreover, newer MRI systems allow faster scanning thus 10-20second temporal sampling can be achieved without a substantial loss in spatial resolution, thus would be prefered over keyhole methods assuming the MRI system is capable to handle the data volume/image reconstruction. To date, we still prefer to perform these functions offline due to data handling restricions on our MRI systems. In addition, we believe motion correction prior to image reconstruction is desirable to reduced motion artifact in subtracted images. This too requires substantial post-processing overhead. Analysis of kinetic properties demonstrated that the rate of enhancement provided greates discrimination of malignant and benign tissues, although overlap of benign / malignant groups remain. These findings are consitent with those of other groups [11]. The amount (amplitude) of enhancement had very little diagnostic value.

Kinetic properties can be combined with tissue/lesion morphology to further enhance specificity of breast MRI. Figure 4 illustrates an example where enhancement rate was

low (i.e. suggesting benign), but morphology shows an irregular lesion border which is suspicios for malignancy - this lesion was invasive ductal carcinoma by pathology. Thus, while morphology was not an emphasis in this project, clearly morphologic and kinetic properties are complimentary.

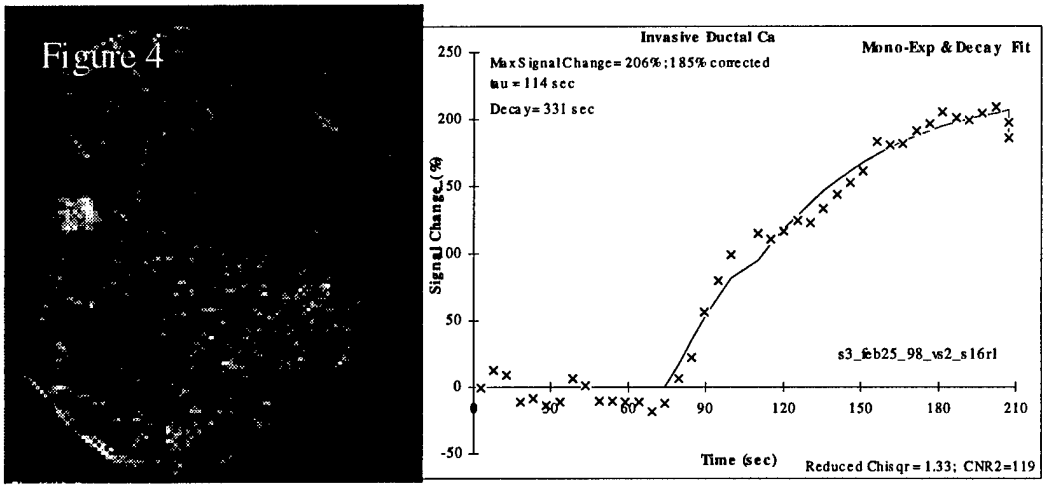

Figure 4: Irregular borders of this lesion suggest a malignancy even though its enhancement rate was low.

In conclusion, high sensitivity of dynamic contrast-enhanced breast MRI, and the ability to detect additional lesions, even in dense breasts, suggests high spatial and high temporal resolution MRI methods will have genuine clinical value. Possible applications include: (1) survey breasts for additional foci prior to surgical biopsy of lesions detected by conventional means; (2) problem-solving imaging in dense tissues or those obscured by implant; (3) means of increased surveillance of women who "test positive" by future serologic or genetic breast cancer screens.

REFERENCES

1. Heywang SH, Hahn D, Schmidt H, et al. MR imaging of the breast using gadolinium-DTPA. J Comput Assist Tomogr 1986; 10(2):199-204.
2. Heywang SH, Wolf A, Pruss E, Hilbertz T, Eiermann W, Permanetter W. MR imaging of the breast with Gd-DTPA: use and limitations. Radiology 1989; 171(1):95-103.
3. Pierce WB, Harms SE, Flamig DP, Griffey RH, Evans WP, Hagans JE. Three-dimensional gadolinium-enhanced MR imaging of the breast: pulse sequence with fat suppression and magnetization transfer contrast. Work in progress. Radiology 1991; 181(3):757-763.
4. Harms SE, Flamig DP, Hesley KL, et al. MR imaging of the breast with rotating delivery of excitation off resonance: clinical experience with pathologic correlation. Radiology 1993; 187(2):493-501.
5. Harms SE, Flamig DP. MR imaging of the breast: technical approach and clinical experience. Radiographics 1993; 13(4):905-912.
6. Heywang-Kobrunner SH. Contrast-enhanced magnetic resonance imaging of the breast. Invest Radiol 1994; 29(1):94-104.
7. Kaiser WA, Zeitler E. MR imaging of the breast: fast imaging sequences with and without Gd- DTPA. Preliminary observations. Radiology 1989; 170(3 Pt 1):681-686.

8. Stack JP, Redmond OM, Codd MB, Dervan PA, Ennis JT. Breast disease: tissue characterization with Gd-DTPA enhancement profiles. Radiology 1990; 174(2):491-494.
9. Orel SG, Schnall MD, Li Volsi VA, Troupin RH. Suspicious breast lesions: MR imaging with radiologic-pathologic correlation. Radiology 1994; 190(2):485-493.
10. Chenevert TL, Helvie MA, Aisen AM, et al. Dynamic three-dimensional imaging with partial K-space sampling: initial application for gadolinium enhanced rate characterization of breast lesions. Radiology 1995; 196:135-142.
11. Quality Determinants of Mammography. Clinical Practice Guide Number 13. USDHHS 1994; AHCPR Publication No. 95-0632.
12. Kuhl CK, Mielcareck P, Klaschik S, et al. Dynamic breast MR imaging: Are signal intensity time course data usefull for differential diagnosis of enhancing lesions? Radiology 1999; 211:101-110.

BIBLIOGRAPHY OF PUBLICATIONS AND MEETING ABSTRACTS SUPPORTED BY THIS GRANT

1. Chenevert TL, Helvie MA, Aisen AM, Francis IR, Adler DD, Roubidoux MA, Londy FL. Dynamic three-dimensional imaging with partial k-space sampling: initial application for gadolinium-enhanced rate characterization of breast lesions. Radiology 1995; 196(1):135-142.

2. Krishnan S, Helvie M, Chenevert TL, Helvie MA, Londy FL. Linear motion correction in 3-dimensions applied to dynamic gadolinium enhanced breast imaging. Med Phys (in press).

3. Chenevert TL, Helvie MA, Aisen AM, Francis IR, Adler DD, Roubidoux MA, Londy FJ. Dynamic Contrast-Enhanced Breast MRI via the 3D Keyhole Technique. Proceedings of the Society of Magnetic Resonance 1994; 1464.

4. Chenevert TL, Krishnan S, Roubidoux MA, Adler DD, Helvie MA. Dynamic Gadolinium Enhancement Characterization of Breast Masses. The DOD Breast Cancer Research Program Meeting Proceedings 1997; 1:227.

5. Chenevert TL, Aisen A, Helvie M, Francis I. Rapid Dynamic Volume MRI for Gad-DTPA Enhancement Quantization of Breast Lesions. Society of Computed Body Tomography and Magnetic Resonance 17th Annual Course; Seattle, WA; April 1994.

PERSONNEL SUPPORTED BY PROJECT:

Thomas L. Chenevert, Ph.D.	Principal Investigator
Mark Helvie, M.D.	Co-Investigator
Marilyn Roubidoux, M.D.	Co-Investigator
Dorit Adler, M.D.	Co-Investigator
Isaac Francis, M.D.	Co-Investigator
Sumati Krishnan	Graduate Student Research Assistant
Frank L. Londy	MRI Technologist
Annette Betley	MRI Technologist, Clinical Coordinator
Chris Lashbrook	Clinical Coordinator
Nancy Thorson	Clinical Coordinator

APPENDIX

Reprint of:
"Dynamic Three-dimensional Imaging with Partial K-Space Sampling: Initial Application for Gadolinium-enhanced Rate Characterization of Breast Lesions"; Radiology 1995; 196: 135-142.

Galley proof of:
Krishnan S, Helvie M, Chenevert TL, Helvie MA, Londy FL. "Linear motion correction in 3-dimensions applied to dynamic gadolinium enhanced breast imaging." Med Phys (in press).

Thomas L. Chenevert, PhD • Mark A. Helvie, MD • Alex M. Aisen, MD • Isaac R. Francis, MD
Dorit D. Adler, MD • Marilyn A. Roubidoux, MD • Frank J. Londy, RTR

Dynamic Three-dimensional Imaging with Partial K-Space Sampling: Initial Application for Gadolinium-enhanced Rate Characterization of Breast Lesions[1]

PURPOSE: **To evaluate a method to monitor gadolinium enhancement patterns at magnetic resonance (MR) imaging with high temporal resolution and full coverage through both breasts.**

MATERIALS AND METHODS: **In 12 patients with 13 masses, including nine carcinoma, nonenhanced three-dimensional MR imaging was performed with full-matrix resolution. At dynamic imaging, 32 serial passes were made during bolus administration of contrast material, and temporal resolution was reduced to 12 seconds by collecting the central (low spatial frequency) 32 × 16 or 16 × 16 phase-encode views. Full-matrix dynamic images were reconstructed by complementing central phase-encode data with precontrast data from peripheral high-spatial-frequency views.**

RESULTS: **Results at time-course analysis with a mono-exponential saturation model indicated malignant lesions tend to show rapid (<60 seconds) contrast change relative to benign masses and normal tissues. One cancer displayed an exceptionally slow contrast change (260 seconds).**

CONCLUSION: **The technical objectives of full tissue coverage, rapid temporal sampling, and quantification of enhancement curves are met with this method for certain lesions (>5 mm in largest diameter).**

Index terms: Breast, MR, 00.12143 • Breast neoplasms, MR, 00.12143 • Magnetic resonance (MR), k-space

Radiology 1995; 196:135–142

EARLY magnetic resonance (MR) imaging demonstrated only limited success in assisting diagnosis of breast disease (1–4). Initially, only tissue-inherent differences in nuclear MR relaxation times, T1 and T2, were the primary sources of contrast. Although these contrasts are relatively high, it was observed that they have little value in helping detection and diagnosis of breast cancer (1,3,5,6). Variable admixtures of intense fat signal and inadequate fat suppression have also seriously hindered image interpretation and detection of breast carcinoma.

More recently, gadolinium-enhanced MR mammography has generated considerable interest (7–10). It is generally accepted that gadolinium enhanced MR imaging offers high sensitivity for the detection of breast cancers. The specificity of gadolinium-enhanced MR mammography to distinguish benign from malignant tissues, however, has been limited by the fact that benign tissues can also exhibit contrast enhancement (9,11,12).

The rate of gadolinium enhancement has also been studied as a potential discriminator of benign and malignant breast neoplasms (13–15). In their initial summary of findings in 25 patients who underwent dynamic gadolinium-enhanced MR imaging, Kaiser and Zeitler reported that all malignancies displayed rapid enhancement (ie, ~100% increase in signal intensity within the first 2 minutes after injection of 0.1 mmol/kg gadopentetate dimeglumine), whereas benign lesions demonstrated less and slower signal intensity change (13). These authors have since updated their dynamic gadolinium-enhanced MR imaging study, in which sensitivity and specificity for cancer detection was greater than 95% (16). In other dynamic gadolinium-enhanced MR imaging studies, higher false-positive rates were observed; thus, there is not a consensus among investigators on methods or diagnostic value of this approach (11,12,17). Findings in these and other studies illustrate that fibroadenomas and proliferative fibrocystic change, in particular, are sources of false-positive findings. Breast malignancies typically exhibit rapid enhancement while benign lesions usually, although not necessarily, exhibit slower contrast change. Malignant lesions may enhance slowly, thus reducing sensitivity (12,18).

Use of various acquisition and enhancement rate quantification schemes may contribute to discrepancies in findings (13–15). In assessment of enhancement rate, important parameters include temporal resolution, volume of tissue covered, and the method used to quantify signal intensity change. In particular, important information on the rate of enhancement may be obscured if the temporal resolution is inadequate to sample rapid contrast changes. In addition, problems will obviously arise if the dynamic imaging volume includes an enhancing lesion only partially or does not include all lesions in the breast. These issues arise in part because there is an inevitable trade-off in standard MR imaging between imaged volume and temporal resolution.

MR imaging with methods such as high spatial resolution, three-dimensional (3D) volumes, suppression of fat signal, and magnetization transfer contrast have been studied in an at-

[1] From the Department of Radiology, University of Michigan Medical Center, 1500 E Medical Center Dr, Ann Arbor, MI 481090030 (T.L.C., M.A.H., I.R.F., D.D.A., M.A.R., F.J.L.); and the Department of Radiology, Indiana University Hospital, Indianapolis (A.M.A.). Received July 28, 1994; revision requested September 14; revision received January 31, 1995; accepted February 6. Supported in part by the National Institutes of Health grant IP30 CA46592, a research award from the Society of Computed Body Tomography and Magnetic Resonance, and U.S. Army grant DAMD17-94-J-4381. **Address reprint requests to** T.L.C.

Abbreviations: ROI = region of interest, 3D = three-dimensional.

The time course of signal change in an ROI of enhancing tissues was fit to a mono-exponential saturation model with use of a Levenberg-Marquardt least-squares optimization algorithm (23). Fitted parameters include contrast onset, t_0; amplitude of signal change, A; and enhancement time constant, τ, used within the following model:

$$\Delta S(t) = \begin{cases} A[1 - e^{-(t-t_0)/\tau}], \text{ for } t > t_0 \\ 0, \text{ for } t \leq t_0. \end{cases} \quad (1)$$

RESULTS

Regarding mass conspicuity, conventional precontrast spin-echo T1- and T2-weighted images frequently did not delineate location or spatial extent of the masses. Visual comparison of pre- versus postcontrast images (T1-weighted spin-echo and gradient-recalled-echo images) was adequate to identify nearly all (12 of 13) palpable and/or mammographically detected masses. Mass detection and localization were facilitated by inspection of anatomic and subtracted cinegraphic images generated by means of the keyhole scheme. Subtraction removed many image features that partially obscured lesions, and cinegraphic display further delineated lesions in terms of time and intensity of contrast change. As the cinegraphic format provided the greatest conspicuity of enhancing tissues, it was used to interactively guide ROI definition on the time-series images. One superficial palpable mass ($\approx$1 cm in largest diameter) displayed signal intensity enhancement, although the enhancement was not distinct relative to surrounding tissues. The mass region was identified as a capsule on the skin that was visible at MR imaging. This mass was occult at conventional x-ray mammography and US and was shown to be benign at pathologic analysis.

Figure 1 illustrates data obtained in a 56-year-old patient with pathologically proved invasive lobular carcinoma in two adjacent sites separated by approximately 1 cm. Mammograms depicted only the larger mass. An early-time-point (ie, before contrast intensity change) keyhole image (Fig 1a) does not depict the two malignant foci, which were most apparent on the late-time-point subtraction keyhole image (Fig 1b). Keyhole matrix size applied in this case was 256 × 32 × 16. Several keyhole subtraction images from the 32-image time series for this section are shown in Figure 1c. While the relatively rapid enhancement period is visually apparent in the time series, temporal contrast patterns of various tissues are best viewed graphically, as shown in Figure 1d. Mono-exponential parameters and fitted curves are also shown in this plot. The time constants of the lesions (τ = 52 or 55 seconds) indicate that the majority of signal intensity change occurs in less than 1 minute. The number or location of these masses was not readily apparent on precontrast images (Fig 1a), although their region roughly correlated with a suspect mass seen on the mammogram.

An example of a slowly enhancing lesion is Figure 2, which was obtained in a 56-year-old patient with a probable fibroadenoma. Findings at MR imaging and mammography were easily correlated for this particular mass, which had been sampled cytologically 7 years earlier. No change in size was seen, as noted in Materials and Methods. A subset of the subtraction-image time series illustrates gradual enhancement of the lesion (Fig 2c). The keyhole matrix size applied in this case was also 256 × 32 × 16. As with the data in Figure 1d, the time-course curve is well fit by an exponential (Fig 2d), although for this lesion the time constant is substantially longer (τ = 119 seconds).

A summary of fitted mono-exponential time constants for a variety of tissue types and all patients is shown in the scatter plot of Figure 3. ROIs from tissues labeled "normal" were derived from areas remote to the mass that displayed sufficient enhancement for curve fitting but were otherwise normal in appearance. These were typically regions of diffuse enhancement from either the ipsilateral or contralateral breast. No more than one normal-tissue ROI was derived in each patient. Two of the five invasive ductal carcinoma tumors were found in one patient (within one breast and separated by approximately 5 cm), and two of the three invasive lobular carcinoma tumors were found in one patient (Fig 1). ROIs of tissues adjacent to invasive ductal carcinoma tumors were defined to avoid signal blur from the lesion focus. As mentioned in Materials and Methods, the keyhole matrix size was 256 × 16 × 16 in three of 12 patients. Masses characterized in these patients were three invasive ductal carcinoma tumors (with largest diameters of 18, 13, and 22 mm and τ of 14, 20, and 18 seconds, respectively) and one neuroendocrine carcinoma (largest diameter, 14 mm; τ, 37 seconds).

There was a clear tendency for the malignant lesions to display rapid contrast changes (τ < 60 seconds) relative to benign or normal tissues. However, one invasive lobular cancer displayed an exceptionally long time constant with τ of 260 seconds. Pathologic examination revealed the tumor had a largest diameter of at least 1 cm (margin was positive at initial biopsy), gross size of 1.2 × 1.0 × 0.8 cm, no angiolymphatic invasion, and no extensive ductal carcinoma in situ; in addition, 17 of 17 lymph nodes were negative for malignancy.

DISCUSSION

We tested a technique with which to perform dynamic, contrast material–enhanced MR imaging of the entire volume of both breasts with a temporal resolution of approximately 12 seconds. The usefulness of the method was explored in our study of 12 patients with a total of 13 breast masses. As found in other studies, we noted a trend for malignant cancers to display rapid enhancement relative to benign and normal tissues, although the presence of one slowly enhancing cancer was observed. This would be considered a false-negative case if the enhancement time constant were used as the sole diagnostic indicator of malignancy. The small number of patients in this study, however, prevents us from drawing statistically meaningful inferences regarding the diagnostic value of this technique. Technical issues aside, other investigators have noted both false-negative and false-positive findings relative to enhancement rate (11,12,17,18).

The viability of this approach for management of breast disease necessitates determination of sensitivity and specificity rates for each application. The role that we are currently evaluating is the contribution of incremental information beyond that provided with conventional imaging modalities when a suspect mass is detected. In this capacity, emphasis is placed on characterization of previously detected masses that are usually more than 5 mm in largest diameter. Lesion localization for eventual dynamic gadolinium-enhanced MR imaging is hindered by nonspecific lesion properties in precontrast MR images and/or by poor correlation of findings with those of other imaging modalities, owing to variable breast geometries and views. This problem is essentially solved with the 3D keyhole approach, which has the inherent features of complete coverage through both breasts and high temporal sampling of dynamic contrast

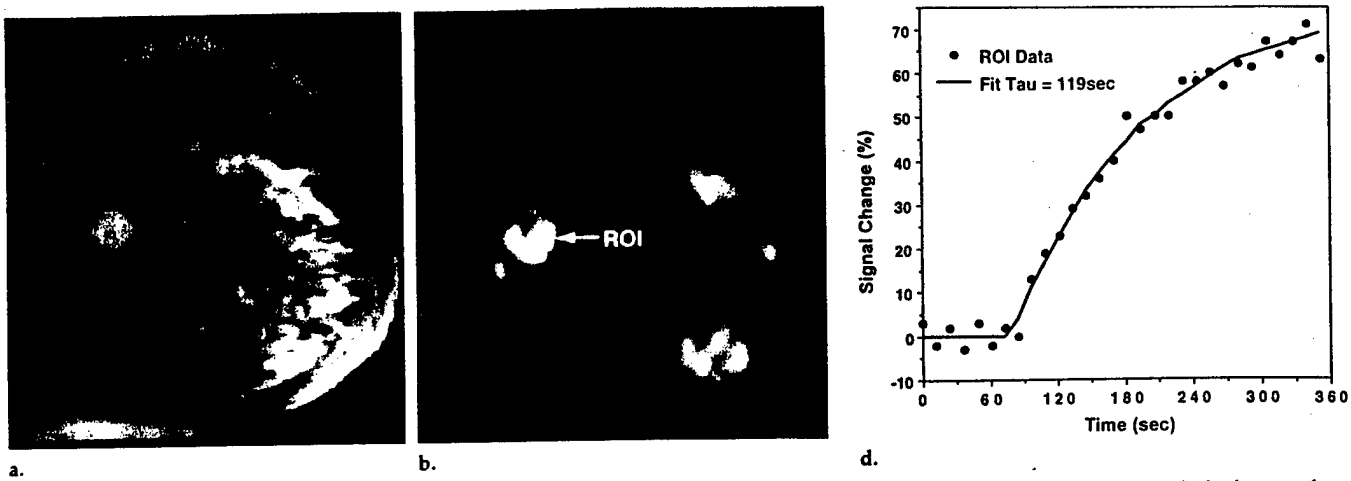

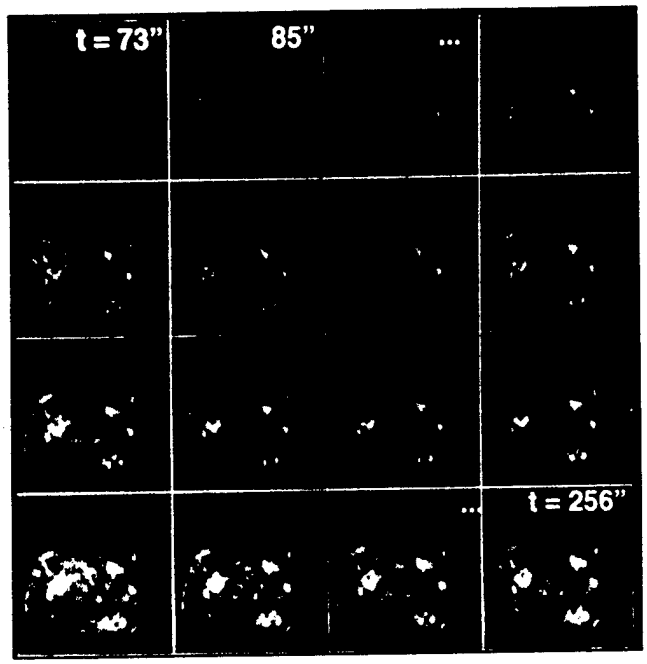

Figure 2. Data from a coronal image obtained through the breast of 56-year-old patient with a stable fibroadenoma. **(a)** Early-time-point (ie, precontrast) keyhole image. **(b)** Subtraction image from a late time point (τ = 355 seconds) of dynamic imaging shows contrast enhancement in the mass *(ROI)*. **(c)** Subset of time series for this section illustrates a gradual contrast change. " = seconds. **(d)** Time-course analysis of the mass indicates that this fibroadenoma has a moderate to long time constant (τ = 119 seconds).

ment properties. An alternative to the keyhole method is rapid acquisition of low-spatial-resolution data sets that are reconstructed and viewed independently from high-resolution data sets. However, we believe the complexities of keyhole reconstruction are justified to ensure the temporal enhancement profiles and spatial properties of a region are correctly related. Spatial blur of enhancement that results from acquisition of limited k space will spread along phase-encode directions to bordering tissue. That is, truly unenhancing tissues can demonstrate apparent enhancement that is actually caused by bleeding of signal intensity from adjacent enhancing tissues. Vertical smearing of signal intensity from small enhancing objects is illustrated in the subtraction images of Figures 1b and 2b.

In addition, the apparent amplitude of enhancement within truly enhanced tissue will be diminished. This effect in the phase-encode dimensions, y and z, is demonstrated with the function that characterizes a uniformly enhancing lesion as

$$\begin{aligned} L(y,z,t) &= L(y,z,0) \cdot [1 + C(t)] \\ &= \mathcal{F}\mathcal{F}^{-1}\{L(k_y,k_z,0) \\ &\quad \cdot [1 + C(t)]\}, \end{aligned} \tag{2}$$

where $C(t)$ defines the temporal properties with $C(0)$ of 0 and $L(k_y,k_z,0)$ describes spatial properties of lesions in k space. Changes in contrast in the reconstructed keyhole image of this lesion, $\mathcal{L}(y,z,t)$, are limited by the spatial frequencies that lie within the sampled keyhole matrix. Thus for $K(k_y,k_z) \equiv 1$ within the keyhole range and zero otherwise, we have

$$\begin{aligned} \mathcal{L}(y,z,t) &= \mathcal{F}\mathcal{F}^{-1}\{L(k_y,k_z,0) \\ &\quad \cdot [1 + K(k_y,k_z) \cdot C(t)]\}. \end{aligned} \tag{3}$$

The apparent enhancement time course of the lesion is derived by multiplying $\mathcal{L}(y,z,t)$ by an ROI mask and then performing spatial integration. The convolution theorem allows us to relate this in k space as

$$\begin{aligned} \Delta ROI(t) &= ROI(t) - ROI(0) \\ &= C(t) \int R(k_y,k_z) \\ &\quad \cdot L(k_y,k_z) \\ &\quad \cdot K(k_y,k_z)dk_ydk_z, \end{aligned} \tag{4}$$

where $R(k_y,k_z)$ is the Fourier transform of the ROI mask. If we assume the spatial pattern of the ROI closely matches that of the enhancing lesion, then $R(k_y,k_z) \approx L(k_y,k_z)$; thus, the integrand becomes $|L(y,k_z)|^2$ within the keyhole area and zero elsewhere. Finally, the full matrix acquisition is used to normalize the contrast suppression effect:

$$\Delta ROI(t) \cong \beta \cdot C(t) \cdot ROI(0);$$

where

$$\beta = \left[\int_{\text{Keyhole area}} |L(k_y,k_z)|^2 dk_ydk_z\right] \div \left[\int_{\text{Full K space}} |L(k_y,k_z)|^2 dk_ydk_z\right]. \tag{5}$$

The factor β represents the degree of suppression in contrast change that results from sampling only a portion of k space. For the above derivation to apply, the time to complete each keyhole pass must be short or must be at least comparable to the period of strong contrast change. The lesion contrast state is considered nearly constant for each keyhole pass but is allowed to vary from pass to pass. While coverage of full k space may

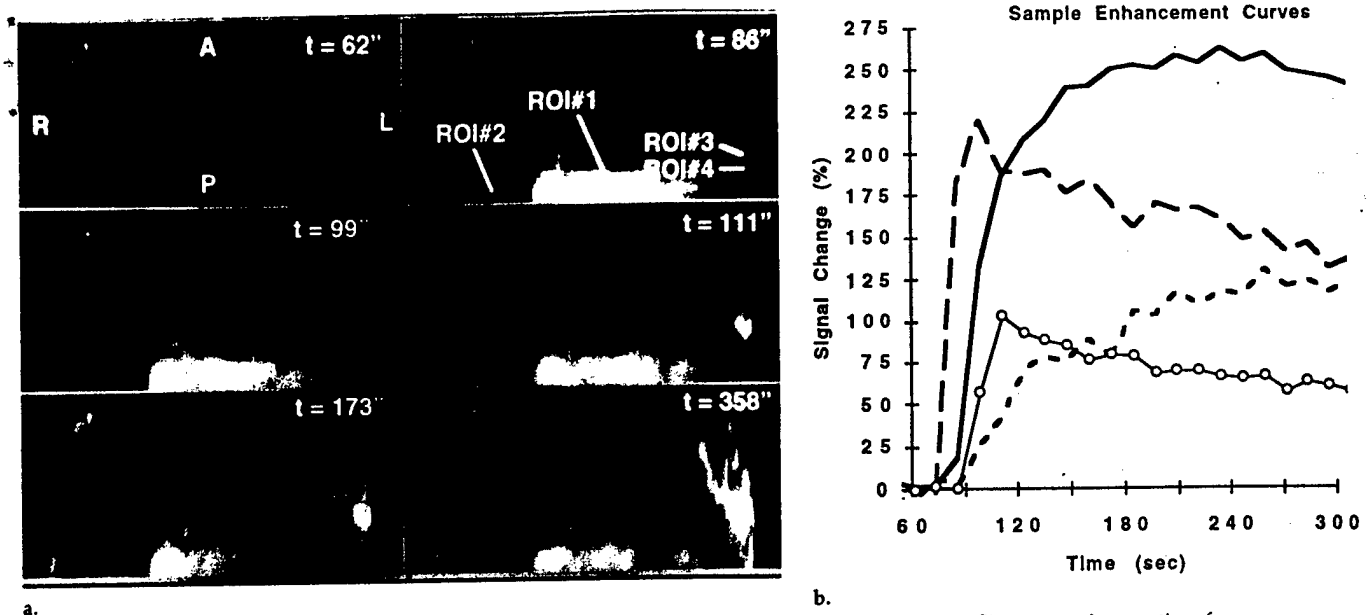

a. b.

Figure 4. **(a)** Maximum intensity projection of subtraction images in the superior-inferior projection. Six noncontiguous time frames are shown from images normally viewed cinegraphically. *ROI#3* delineates an invasive ductal carcinoma. Enhancement in linear structures delineates vessels. *A* = anterior, *L* = left, *P* = posterior, *R* = right, *t* = time (seconds). " = seconds. **(b)** Corresponding enhancement-time-course curves for ROIs 1–4 illustrate changes in relative rate and intensity of enhancement. Curves were derived from ROIs drawn on related single-section cinegraphic displays. *ROI#1* = left ventricular blood (broken line), *ROI#2* = liver (O), *ROI#3* = invasive ductal carcinoma (solid line), *ROI#4* = area adjacent to mass (dashed line).

across these studies. The immediate technical objectives of this study were to overcome these critical limitations. These objectives are largely met with the 3D keyhole technique, which offers full tissue coverage at high temporal sampling for subsequent quantitative enhancement time characterization. As we have discovered, the ability to dynamically study entire breasts at MR imaging, thus obviating prospective identification of one or all lesions amidst complex contrasts, is a great practical advantage. A drawback of this approach is the large data volume generated per case. Currently, we resolve the data management issue by performing reconstruction, display, and analysis on an off-line workstation with customized software tools. Our software has been specifically designed to present data in a variety of formats for specific purposes, such as the survey of all tissues in cinegraphic maximum-intensity-projection images of subtraction images or the cinegraphic viewing of a single section for quantitative analysis of individual tissues. This method also benefits from the other well-known features of breast MR imaging, such as the ability to image breasts with dense parenchyma or implants and to provide high-quality reformatted tomographic views that can potentially aid planning for surgery. ■

Acknowledgment: The authors thank James Pipe, PhD, for providing assistance with Advanced Visual Systems software.

References

1. Stelling CB, Powell DE, Mattingly SS. Fibroadenomas: histopathologic and MR imaging features. Radiology 1987; 162:399–407.
2. Turner DA, Alcorn FS, Adler YT. Nuclear magnetic resonance in the diagnosis of breast cancer. Radiol Clin North Am 1988; 26:673–687.
3. el Yousef SJ, O'Connell DM, Duchesneau RH, Smith MJ, Hubay CA. Benign and malignant breast disease: magnetic resonance and radiofrequency pulse sequences. AJR 1985; 145:1–8.
4. Heywang SH, Fenzl G, Hahn D, et al. MR imaging of the breast: comparison with mammography and ultrasound. J Comput Assist Tomogr 1986; 10:615-620.
5. Heywang SH, Bassermann R, Fenzl G, et al. MRI of the breast: histopathologic correlation. Eur J Radiol 1987; 7:175-182.
6. Wiener JI, Chako AC, Merten CW, Gross S, Coffey EL, Stein HL. Breast and axillary tissue MR imaging: correlation of signal intensities and relaxation times with pathologic findings. Radiology 1986; 160:299–305.
7. Heywang SH, Hahn D, Schmidt H, et al. MR imaging of the breast using gadolinium-DTPA. J Comput Assist Tomogr 1986; 10:199–204.
8. Heywang SH, Wolf A, Pruss E, Hilbertz T, Eiermann W, Permanetter W. MR imaging of the breast with Gd-DTPA: use and limitations. Radiology 1989; 171:95–103.
9. Pierce WB, Harms SE, Flamig DP, Griffey RH, Evans WP, Hagans JE. Three-dimensional gadolinium-enhanced MR imaging of the breast: pulse sequence with fat suppression and magnetization transfer contrast—work in progress. Radiology 1991; 181:757–763.
10. Harms SE, Flamig DP, Hesley KL, et al. MR imaging of the breast with rotating delivery of excitation off resonance: clinical experience with pathologic correlation. Radiology 1993; 187:493–501.
11. Harms SE, Flamig DP. MR imaging of the breast: technical approach and clinical experience. RadioGraphics 1993; 13:905–912.
12. Heywang-Kobrunner SH. Contrast-enhanced magnetic resonance imaging of the breast. Invest Radiol 1994; 29:94–104.
13. Kaiser WA, Zeitler E. MR imaging of the breast: fast imaging sequences with and without Gd-DTPA. I. Preliminary observations. Radiology 1989; 170:681–686.
14. Stack JP, Redmond OM, Codd MB, Dervan PA, Ennis JT. Breast disease: tissue characterization with Gd-DTPA enhancement profiles. Radiology 1990; 174:491–494.
15. Hachiya J, Seki T, Okada M, Nitatori T, Korenaga T, Furuya T. MR imaging of the breast with Gd-DTPA enhancement: comparison with mammography and ultrasonography. Radiat Med 1991; 9:232–240.
16. Kaiser WA. MR mammography. Radiologe 1993; 33:292–299.
17. Orel SG, Schnall MD, Li Volsi VA, Troupin RH. Suspicious breast lesions: MR imaging with radiologic-pathologic correlation. Radiology 1994; 190:485–493.
18. Schnall MD, Orel S, Muenz L. Analysis of time intensity curves for enhancing breast lesions (abstr). In: Proceedings of the Society of Magnetic Resonance in Medicine 1993. Berkeley, Calif: Society of Magnetic Resonance in Medicine, 1993; 120.
19. Harms SE, Flamig DP, Hesley KL, et al. Fat-suppressed three-dimensional MR imaging of the breast. RadioGraphics 1993; 13:247–267.
20. van Vaals JJ, Brummer ME, Dixon WT, et al. "Keyhole" method for accelerating imaging of contrast agent uptake. J Magn Reson Imaging 1993; 3:671–675.
21. Chenevert TL, Pipe JG. Dynamic 3D imaging at high temporal resolution via reduced k-space sampling (abstr). In: Proceedings of the Society of Magnetic Resonance in Medicine. Berkeley, Calif: Society of Magnetic Resonance in Medicine, 1993; 1262.
22. Spraggins TA, de Paredes ES, De Angelis GA, Thiele F. Three keyhole imaging: ap-

Linear motion correction in three dimensions applied to dynamic gadolinium enhanced breast imaging

Sumati Krishnan, Thomas L. Chenevert,[a] Mark A. Helvie, and Frank L. Londy
1500 E. Medical Center Drive, Department of Radiation Oncology, University of Michigan Hospitals, Ann Arbor, Michigan 48109

(Received 8 May 1998; accepted for publication 24 February 1999)

Quantitative analysis of dynamic gadolinium-DTPA enhanced MRI is emerging as a highly sensitive tool for detecting malignant breast tissue. Three-dimensional rapid imaging techniques, such as keyhole MRI (magnetic resonance imaging), yield high temporal sampling rates to accurately track contrast enhancement and washout in lesions over the course of multiple volume acquisitions. Patient motion during the dynamic acquisitions is a limiting factor that degrades the image quality, particularly of subsequent subtraction images used to identify and quantitatively evaluate regions suggestive of malignancy. Keyhole imaging is particularly sensitive to motion since datasets acquired over an extended period are combined in *k*-space. In this study, motion is modeled as set of translations in each of the three orthogonal dimensions. The specific objective of the study is to develop and implement an algorithm to correct the consequent phase shifts in *k*-space data prior to offline keyhole reconstruction of images of 3D volume breast MR acquisitions. © *1999 American Association of Physicists in Medicine.* [S0094-2405(99)01005-6]

Key words: breast, neoplasms, keyhole, linear motion, post-processing algorithms

INTRODUCTION

Contrast enhanced MRI is a developing technique for characterization of breast lesions.[1–8] This method is based on the tendency of lesions to exhibit enhancement after administration of gadolinium-based contrast media. Furthermore, malignant tissues typically exhibit rapid enhancement due to anomalous vascularity, in which the combination of increased capillary density and permeability results in rapid enhancement, and occasionally washout, of the contrast agent in a dynamic contrast MRI study.[9–12] Benign tissues, on the other hand, tend to have a slower enhancement rate.[5] Some benign tissues, such as fibroadenomas, have been observed to exhibit rapid enhancement,[13] thereby reducing the specificity of dynamic contrast enhanced MRI of the breast. Nevertheless, analysis of the temporal enhancement patterns is considered an emerging tool that can be used for detection and differentiation of various breast lesions. For this purpose, two-dimensional multisection breast MR imaging has been performed with an associated temporal resolution of ~1 min.[5] Even better temporal resolution (15 s) has been achieved by imaging one or a few pre-selected slices.[7] Realistically, selection of a few slices based on findings at x-ray mammography, ultrasonography, or physical examination can be difficult and is useful only in characterizing known lesions. Correlation of these findings to a few MRI imaging slices is difficult due to the variable deformation of the breast. Also, since certain lesion are not easily identified in the absence of contrast agents, a precontrast MR image by itself could prove inadequate for prospective selection of appropriate imaging sections. Thus for dynamic MR breast imaging to be a useful screening tool, techniques that provide 3D volume images of one or both breasts while sampling contrast enhancement information at high temporal resolution, are desired.

Three-dimensional dynamic MRI consists of acquiring serial 3D volume images over a finite time period that encompasses contrast enhancement. The time per acquisition is a function of the imaging parameters, such as matrix size, number of excitations (NEX), and the type of acquisition sequence used.[14] Three-dimensional volume imaging with fat suppression using magnetization transfer contrast has been performed to yield images of good anatomic quality, i.e., high spatial resolution, but with acquisition times ranging to several minutes.[15] Rapidly enhancing tissues have been observed to reach peak enhancement on the order of tens of seconds. To be sensitive to the most rapidly enhancing tissues high sampling rates are required which is achieved, in part, by using fast imaging techniques, such as a 3D fast rf-spoiled gradient recalled echo (3D SPGR) sequence used in this study. Despite improvements in the speed of the imaging pulse sequence, there remains a tradeoff between high spatial resolution and high temporal sampling rates, which relates to the objective of breast lesion detection and characterization. One approach to address this tradeoff has been to subsample *k*-space using a tailored traversal pattern, while maintaining a high dynamic temporal sampling rate. The resulting spatial resolution usually depends upon the extent of *k*-space traversal and the reconstruction algorithm. Examples include reduced-encoding imaging using generalized reconstruction (RIGR),[16] use of projection reconstruction trajectories,[17] and dynamic spiral breast imaging.[18] A particular technique, used for data acquisition in this study, that similarly mitigates the spatial-

 0094-2405/99/26(5)/1/8/$15.00

temporal tradeoff is the "keyhole" MRI technique described in the following section.

The keyhole technique involves the acquisition of one or more reference high-resolution datasets followed by a dynamic series of datasets having a limited extent in k-space.[19] The reduced matrix acquisition usually samples only the central portion of k-space, which is then spliced with peripheral k-space data from a full matrix reference dataset acquired initially. In keyhole acquisitions it is assumed that the significant dynamic events (such as amplitude changes in breast lesions), are tracked by acquiring the central k-space lines. The adequacy of tracking changes depend on the spatial features of the enhancing object. It is an inherent limitation of keyhole imaging that features exhibiting temporal enhancement will be blurred by an amount dependent on the keyhole matrix size and the spatial dimensions of the object. Fine structures with a higher peripheral spatial frequency content will be blurred by a greater amount.[20] However, the spatial detail of static, nonenhancing, background structures is restored by splicing together the high spatial frequencies from the reference dataset. This serves to provide a high-resolution anatomic context for evaluating the dynamically changing lesions.[21]

A significant source of error related to keyhole imaging will be due to breast motion over the total acquisition period. This will manifest as phase differences between the reference and dynamic datasets. For contrast enhanced MRI, quantitative analysis is commonly performed on subtraction images that emphasize temporal changes. Keyhole reconstruction of the phase-deviant datasets will result in substantial edge artifacts and blurring in the subsequent subtraction images used for quantitative analysis.[22] A number of motion models and corresponding post-processing techniques have been proposed to reduce motion artifact for two-dimensional Fourier transform imaging.[23–27] The purpose of this paper is to outline a 3D model for motion during the rapid dynamic acquisition and describe a method of estimation and correction for the phase artifacts introduced by motion. The motion correction algorithm was initially verified by computer simulation. It was tested on a phantom experiment dataset and applied to clinical breast studies.

MATERIALS AND METHODS

Motion correction

Dynamic breast imaging data was acquired using a dual phased array coil, which permitted processing of data from the right and left coils separately. Thus motion correction was applied individually to each breast. The motion model was based on a consideration of the patient configuration and imaging rates. With some mild compression most patients were reasonably well constrained within the breast coil. The 3D SPGR imaging sequence acquired a single 3D volume once every ~10 s. Since the patients were cautioned to hold still, the most likely causes of motion were gradual positional shifts that evolved on a time scale longer than the dynamic temporal sampling rate. Thus, we assume negligible intrakeyhole motion and consider a mean position over each dynamic volume acquisition. Based on visual inspection of the subtraction edge artifacts observed, we further limit our analysis to simple translations in each of the three orthogonal dimensions. Our primary focus, therefore, was to detect and correct simple displacements that occurred over the duration of the overall dynamic acquisition on a per keyhole basis. Thus, the model assumed that after the reference acquisition and between each subsequent dynamic acquisition, the individual breasts were allowed to move independently as rigid bodies undergoing only translational motion.

It is known that a simple displacement in space introduces a corresponding phase shift in the spatial frequency signal while the magnitude of the data remains unchanged.[28] Thus there is a phase difference between the reference dataset and the dynamic dataset acquired after the object has been displaced. Let $S(k_x,k_y,k_z)$ represent the reference dataset in the spatial frequency domain, given by

$$S(k_x,k_y,k_z)=\int \rho(x,y,z)^{e(i(k_xx+k_yy+k_zz))}dxdydz. \quad (1)$$

Now, let the object, $\rho(x,y,z)$, be displaced by Δx, Δy, Δz at a given time point. The new position of the object can be described as a convolution with a displaced delta function

$$\rho'(x,y,z)=\rho(x,y,z)\otimes\delta(x-\Delta x,y-\Delta y,z-\Delta z). \quad (2)$$

Consequently, the k-space data from the object is now given by

$$S'(k_x,k_y,k_z)=S(k_x,k_y,k_z)^{e(-i(k_x\Delta x+k_y\Delta y+k_z\Delta z))}. \quad (3)$$

Thus the net phase shift due to 3D translation is given as

$$\phi(k_x,k_y,k_z)=k_x\Delta x+k_y\Delta y+k_z\Delta z. \quad (4)$$

In keeping with our motion model, the objective of the motion correction algorithm was to estimate this linear phase shift of the entire keyhole k-space block relative to the reference data block per spatial frequency axis, and apply a phase correction to each dataset prior to keyhole reconstruction. The approach was to compute an averaged linear phase roll along each individual k-space axis, [Eq. (5)] which is in effect a projection of mean phase difference over the 3D dataset, onto that particular axis.

To implement the algorithm, first a phase difference matrix was generated between a central (32×32×32) kernel extracted from the reference dataset and each dynamic time point. The phase difference was estimated on reduced matrix spatial frequency datasets, because it cannot be reliably computed in the low amplitude, peripheral k-space, regions of the signal. In these regions the noise amplitude is comparable to that of the signal and hence the phase could fluctuate randomly, obscuring the effect of linear motion. The average phase difference along each spatial frequency axis was computed as follows:

$$\phi(k_x)=\frac{1}{(n_y\cdot n_z)}\sum_{\downarrow k_y}\sum_{\downarrow k_z}\cdot\phi(k_x,k_y,k_z) + \text{constant term},$$

$$\bar{\phi}(k_y)=\frac{1}{(n_x\cdot n_z)}\sum_{\downarrow} k_x \sum_{\downarrow} k_z\cdot\phi(k_x,k_y,k_z) + \text{constant term}, \quad (5)$$

$$\phi(k_z)=\frac{1}{(n_x\cdot n_y)}\sum_{\downarrow} k_x \sum_{\downarrow} k_y\cdot\phi(k_x,k_y,k_z) + \text{constant term},$$

where, n_x, n_y, n_z, is the matrix size and, $\phi(k_x)$, $\phi(k_y)$, $\phi(k_y)$, are the averaged phase deviations per k-space axis.

Thus we obtain a phase difference function per k-space axis which is a measure of the averaged phase difference between the reference and dynamic datasets, due to displacement in the corresponding spatial axis during a particular dynamic timepoint. For example, in Fig. 1(a) the coronal plane image shows a noticeable edge artifact. Figure 1(b) in turn, shows a net averaged linear phase roll detected along the k_x and k_z dimensions and negligible phase deviations in k_y. This implies linear displacement along the x and z dimensions. Thus the phase function is an estimate of the translation induced phase shift. The linear phase function could contained wrapped phase depending on the extent of motion along a particular spatial axis. Thus, an unwrapping algorithm was applied to each function so that it increased or decreased monotonically. These averaged phase deviation functions were submitted to a linear least squares estimation algorithm from which a representative slope per spatial frequency axis was computed. This slope was used to correct the phase deviant dataset by simply applying an inverse linear phase ramp such that

$$\phi_{\text{corr}}(k_x,k_y,k_z)=k_x s_x+k_y s_y+k_z s_z, \quad (6)$$

where, s_x, s_y, and s_z were the fitted slopes in k_x, k_y, and k_z.

The constant phase shift term between the reference and the slope-corrected datasets was also determined and incorporated in the phase correction algorithm. In the case of very large displacements [$>\frac{1}{2}$ (FOV) field of view] along each axis, the phase difference function could be wrapped twice. The unwrapping technique used would not be able to account for this in a single stage and hence the correction algorithm was applied to the data in two consecutive stages.

ANALYSIS OF AMPLITUDE MODULATION EFFECTS

The amplitude modulation of the data that is associated with uptake of Gd-DTPA could theoretically, be misinterpreted as a phase shift. Computer simulations were used to further analyze this effect. We investigated the effect of signal enhancement by considering signal increases starting from 100 to a maximum of 500 percent. Two simplified anatomic configurations of breast fat and lesion were considered. First, we varied the percentage of simulated lesion area to breast fat area from 1%–60%. We increased lesion size relative to the size of the background fat while changing the

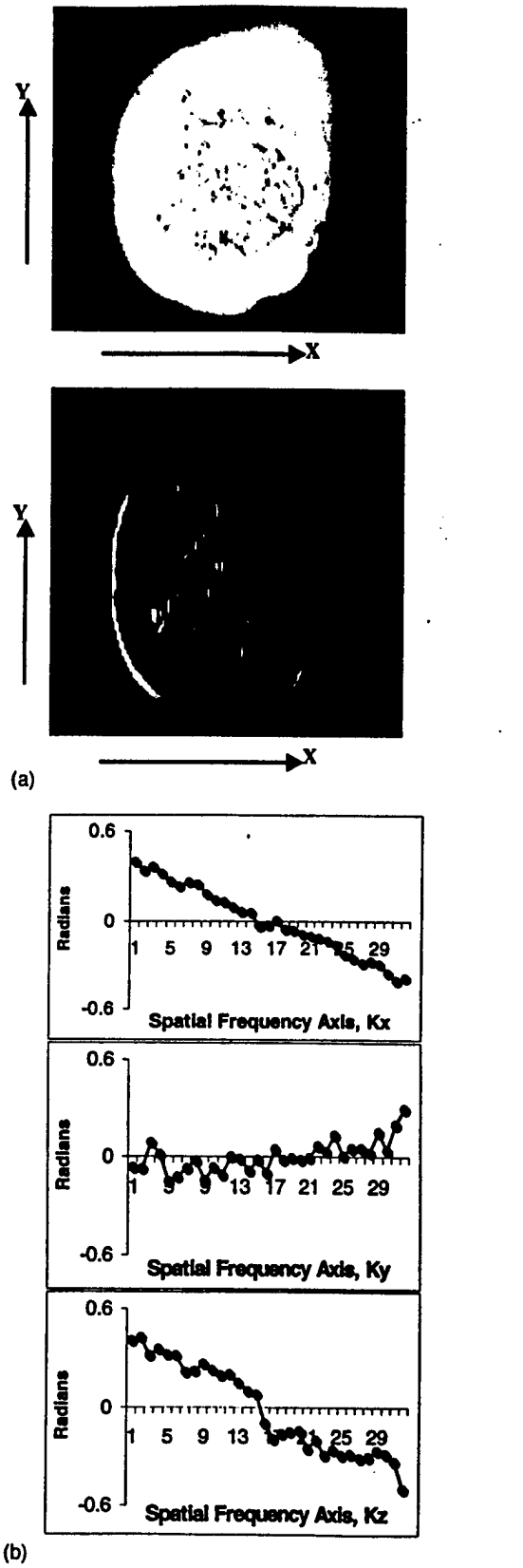

FIG. 1. (a) Reconstructed image of single (right) breast after separating dual phased array data. Bottom image shows representative subtraction artifact on coronal slice of dynamic timepoint 14. (b) Averaged phase deviations per spatial frequency axis for dynamic timepoint shown in (a), relative to the reference dataset.

percent signal enhancement within the lesion. The phase difference between each enhanced and the original unenhanced dataset was computed. Second, we varied the displacement between the axes of the simulated breast fat and lesion from 0 to 5 cm. We displaced breast fat relative to a fixed lesion. Again, for each axial displacement configuration the percent signal enhancement was varied and the phase difference between the enhanced and unenhanced datasets was computed.

MR imaging

The breast studies were performed on a 1.5*T* system (General Electric Medical Systems, Milwaukee, Wisconsin), using a dedicated breast dual phased array coil. For the clinical data, *T*1 and *T*2 weighted axial scans were performed initially. A pre-contrast coronal reference dataset was acquired using the locally developed 3D fast rf-spoiled GRE (3D SPGR) sequence, 40 degree flip angle. Imaging parameters were a TR/TE of ~13/5 ms, acquisition matrix, 256 ×128×32 with 3–5 mm thick sections and four excitations. The field of view (FOV) ranged from 28 to 36 cm (typically 32 cm). The dynamic contrast-enhanced series consisted of 20 serial 3D volumes acquisitions with a reduced matrix of 256×32×32 and single excitation, followed by one full matrix dataset. The dynamic segment spanned ~5 min during which a bolus injection of Gd-DTPA was administered within the first 30–45 s of the scan, at a dose of 0.1 mmol per kilogram body weight. Each dynamic 3D dataset was acquired at 12.3 s intervals, which is equivalent to the overall temporal resolution. Finally a series of post-contrast coronal 3D SPGR and an axial *T*1 weighted scan were performed.

Keyhole reconstruction of the data was performed offline using custom software programs developed in AVS (Advanced Visual Systems Inc., Waltham MA). The low spatial frequencies from each dynamic dataset were spliced into the reference dataset to create the corresponding full matrix dynamic dataset, for subsequent 3D Fourier transform reconstruction. Cinegraphic loops of reconstructed anatomic and subtraction images were reviewed on the workstation. A precontrast time point was used as the subtraction mask.

Phantom studies

The motion-correction algorithm was calibrated experimentally. Displacements were introduced in each of the three spatial axes using a lever arm rigidly attached to the experimental phantom located in the breast coil. Motion was induced by translating the lever arm over a calibration scale such that the phantom was displaced by an exact amount, in increments of 2 mm. The maximum displacements introduced were 2 cm along the *x* and *y* axes, and 1 cm along the *z* axis.

The 3D dynamic simulation experiment was performed on a breast-mimicking phantom, on the 1.5*T* GE system. Mineral oil was used to simulate breast fat and water to simulate breast parenchyma in each of the phantom compartments. Motion was induced in only one breast phantom compartment by raising and laterally displacing a lever attached to the phantom. Motions were designed to simulate the slow

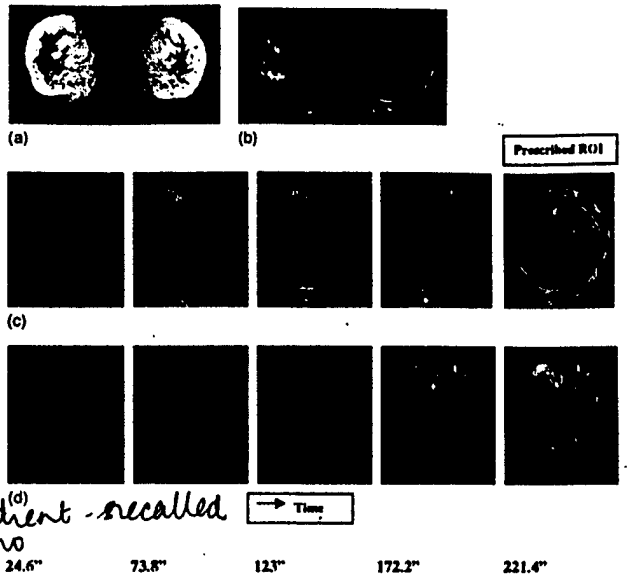

FIG. 2. Coronal slice of 3D volume acquisition (a). Anatomic image of uncorrected coronal slice. (b) Subtraction image of the same slice with clearly visible subtraction edge artifact. (c) Time series of edge artifact in the same slice prior to motion correction, 49.2 s intervals. (d) Time series of edge artifact in the same slice after motion correction, 49.2 s intervals.

displacement commonly observed over the duration of the scan. Uptake of contrast in a lesion was simulated by injection of 10 cc of 2 mmol Gd-DTPA into 5 cc vials located in each breast phantom compartment.

Patient studies

The clinical data included 64 breast patients who were scanned as part of an ongoing research project. Study population consisted of patients with abnormal mammograms or ultrasonically detected suspicious masses who were referred for MR scans. Patients were scanned prone with their breast suspended in the coil. Mild compression was applied to the breasts but no rigid immobilization techniques were employed. The standard clinical procedure was to caution the patients to hold still during and in between scans.

Quantitative assessment

The effectiveness of the motion correction algorithm was quantitatively assessed by comparing subtraction edge artifact prior to and after motion correction. A single measure that summarized edge artifact was devised and computed by the following procedure. For each of the 64 breast cases a representative mid-breast slice was chosen. Based on the subtraction images, a single ROI encompassing all of the noticeable motion artifact induced edge was defined (Fig. 2). This ROI was used as a mask over the entire sequence of dynamic timepoints and a mean ROI intensity per time point was computed, for the corrected and uncorrected datasets at the selected slice of interest. Next a baseline value equal to the mean ROI intensity from the second time point in a series was subtracted off from all other time points, providing the desired estimate of subtraction edge artifact. This temporal

series of mean artifact ROI's was further approximated to a single mean and peak artifact ROI over the entire dynamic acquisition. Similar mean ROI's intensities were calculated for a region in each dynamic time point that corresponded to the background noise signal, for both corrected and uncorrected datasets. In order to compare the edge artifact correction across patients, the artifact ROI intensities were normalized by the mean background noise ROI intensity.

RESULTS

The calibration experiment for the motion correction algorithm yielded the following results. The correlation coefficient between the induced and detected displacements was 0.999 for the x, y, and z dimensions. Thus, there was a close overall agreement between the induced and detected displacement along each of the spatial axes. A minimum displacement of 2 mm was induced and detected along each spatial axis. The theoretical limit to the maximum displacement that could be corrected for, is equivalent to a half field of view along that particular spatial axis.

The phase slopes in k_x, k_y, and k_z measured in the 3D dynamic experimental data, corresponded to a maximum displacement of ~6 mm along the anterior–posterior direction (A/P), 2 mm along the right–left (R/L) direction and negligible motion along the superior–inferior (S/I) direction. Figure 3 demonstrates the effect of motion correction on the phantom. A marked reduction in motion-induced blurring and ghosting was observed on the subtracted and nonsubtracted images. An overall improvement in the edge artifact at breast boundaries as well as good background suppression was achieved for the motion-corrected subtraction images. It is interesting to note that after motion correction the vial on the right [Fig. 3(d)] is no longer visible. This is because the vial is truly outside the level of the selected slice in the 3D volume. It is visible on the uncorrected image due to subtraction artifact. After motion correction the slice is reregistered to the appropriate cross sectional level.

There was no significant difference in the mean ROI computed for each vial due to motion correction compared to the dataset without motion correction. This result was expected since the size of the simulated lesion was fairly large and therefore keyhole imaging could accurately track dynamic changes.

The simulation investigating the effect of contrast modulation on phase estimation showed enhancement effects to be negligible. We found that, as long as the high signal unenhancing breast fat, was larger in area or mostly coaxial with the enhancing lesion, the phase deviations were very small for all conditions of enhancement within the lesion. The computed phase errors were negligible for lesion as large as 60% of breast area with axial separations up to 5 cm. This was validated by the phantom experiment where the lesion-simulating vial was small compared to the breast fat compartment and located coaxially. There was no significant difference between the mean ROI in the signal enhancing vial without motion, and the post-correction mean ROI in the signal enhancing vial with induced motion. This implies that the motion-correction phase estimates were computed accurately in the contrast-enhanced displaced datasets. Additionally, in a couple of patient datasets we observed substantial enhancement in the breast parenchyma with contrast administration, however motion correction did not result in a mispositioning of this enhancing parenchyma, since it is mostly coaxial with breast fat.

There were a range of results for the clinical breast data, depending on the nature of the motion that might have occurred during the exams. For a typical study we maintained a 32 cm FOV with 4 mm thick slices at a (256×32×32) matrix size. At these settings the maximum detected slopes, over all patients, corresponded to a displacement of 8, 5, and

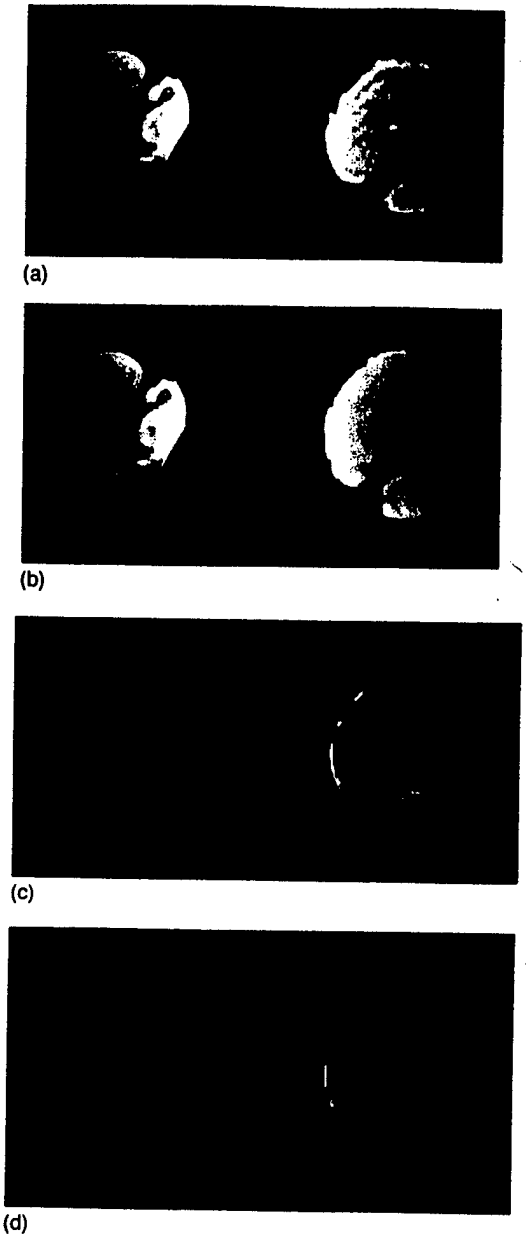

FIG. 3. Phantom experiment with breast mimicking phantom, coronal slice of 3D volume. (a) Unsubtracted original image. (b) Unsubtracted image after motion correction. (c) Subtraction image prior to motion correction. (d) Subtraction image after motion correction.

3 mm in A/P, S/I, and R/L directions, respectively.

Qualitative visual assessment of the subtraction images showed that in certain cases there was substantial observable motion artifact in the uncorrected datasets, that was successfully removed in the corresponding motion-corrected images. The improvement was most noticeable as a marked reduction in subtraction edge artifact. Low amplitude ghost artifact and blurring in the background was also substantially reduced (Fig. 4). This effect was noticed by the improved clarity of features such as the nipples. Motion correction also enhanced the visual quality of fine structures such as vessels seen in axial and cross-sectional orientations (Fig. 2). From the plots of mean slope per time point in Fig. 4, we see that the motion correction algorithm has the freedom to individually correct each breast. In this example, greater displacements were detected for the right as compared to the left breast, providing the same overall degree of correction for both breasts.

Quantitative analysis of motion artifact reduction for the clinical cases is summarized in Fig. 5. The mean subtracted artifact ROI intensity over all dynamic timepoints, normalized to the background noise signal intensity, motion corrected vs uncorrected datasets, is plotted in Fig. 5(a). The corresponding plot for the peak artifact ROI is shown in Fig. 5(b). The line of unity represents equivalent artifact in motion corrected and noncorrected datasets. The filled circles in the graphs [Figs. 5(a) and 5(b)] correspond to the peak and mean artifact correction levels for the edge artifact seen in Fig. 4. For this representative artifact we see that there was a roughly 40% reduction in subtraction edge artifact, resulting in the improved visibility described earlier. We can summarize the results of motion correction in terms of the edge artifact measure as follows:

Motion correction produced a reduction in mean artifact ROI in a number of cases, i.e., there was an improvement in edge artifact suppression. For certain cases there was no significant difference between the mean ROI's for the corrected and uncorrected datasets. This suggests that other sources of phase artifact, such as rotations and distortions, that did not fit the linear three-dimensional translational model, could be present. In none of the cases was the mean artifact ROI greater for the motion corrected dataset compared to the uncorrected dataset. This implies that the correction algorithm did not introduce any additional artifact.

CONCLUSIONS AND DISCUSSION

Contrast enhanced MRI is developing into a fairly useful tool for the detection and characterization of breast tumors. The potential for breast MRI as a clinical diagnostic tool lies in the ability to achieve volume imaging of both breasts at high spatial resolution, yielding good anatomic detail. In addition contrast enhanced dynamic imaging provides functional information that could assist in tumor characterization. The fidelity of the MRI image data is often limited by artifact sources including motion during the acquisition.

In keyhole substitution MRI an effect of linear motion is to introduce phase discontinuities and shifts between the dynamic and reference datasets. These phase deviations manifest as edge artifacts and cause blurring, rather than an observable gross displacement, of small lesions in subtraction images that are used for quantitative analysis. This is because the bulk (three fourths) of the spatial information is


(a)


(b)

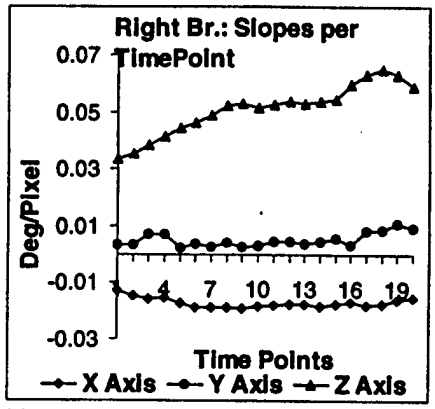

(c)

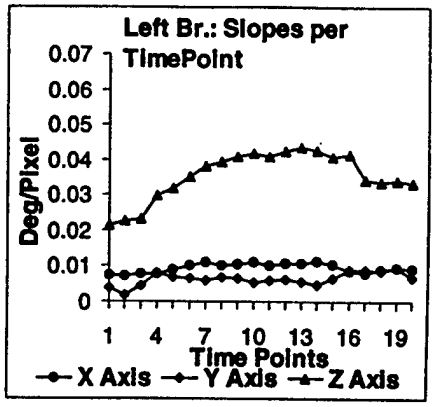

(d)

FIG. 4. Coronal slice of 3D volume acquisition. (a) Subtraction image before motion correction. (b) Subtraction image after motion correction. Note improved clarity of nipples (arrow) and reduced subtraction edge. (c) Mean slopes in k_x, k_y, and k_z per time point in left breast. (d) Mean slopes in k_x, k_y, and k_z per time point in right breast.

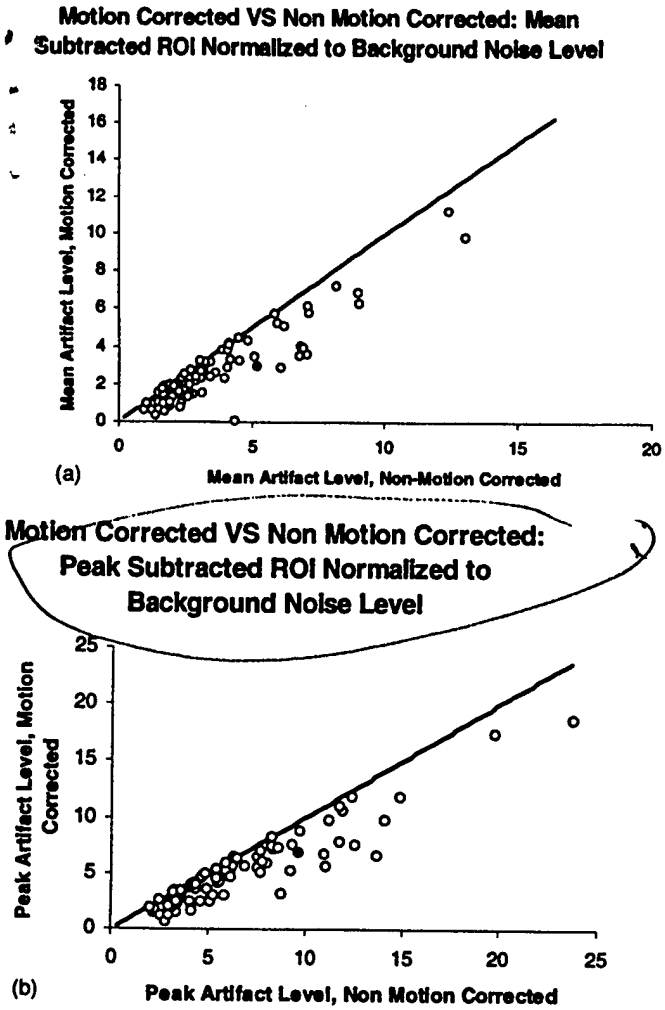

FIG. 5. (a) Comparison of mean artifact level per dynamic series between motion-corrected and uncorrected datasets. (b) Comparison of peak artifact level per dynamic series in motion-corrected and uncorrected datasets.

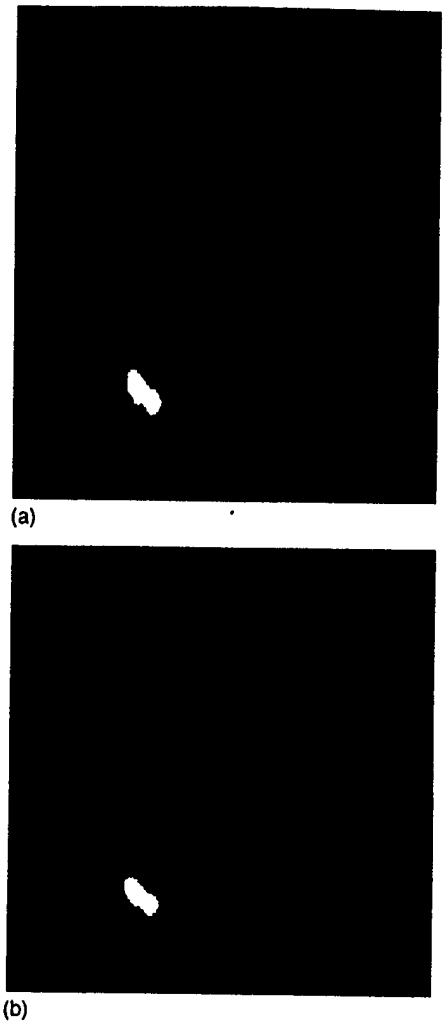

FIG. 6. Example of subtraction edge due to keyhole reconstruction of motion corrupted dataset, while contrast information is retained. (a) Uncorrected coronal slice, showing malignant lesion and broad subtraction edges. (b) Same slice after correction, showing reduction in edge artifact, while maintaining lesion clarity and contrast. The detected displacements were 1.6, 4.7, and 8.1 mm along the x, y, and z axes.

derived from the peripheral high frequencies in the reference dataset. Figure 6 is an illustration of this effect. We observe that motion produces subtraction edge artifact and some amount of lesion blurring, but retains most of the lesion contrast information. The artifacts can, however, obscure lesions or result in reduced visibility in subtraction images that normally offer the greatest lesion conspicuity. Superficial lesions that lie near high contrast boundaries could remain undetected. Furthermore, identifying lesion ROI's in these artifactually blurred images could lead to inaccurate quantification of contrast uptake characteristics. Thus, effective motion correction algorithms are desirable in contrast-enhanced breast MRI.

The scope of this study was limited to gross translational rigid body motion of the breast. The motion correction algorithm assumes no intrakeyhole motion, i.e., motion during the acquisition of a single dynamic block. In this context, calculating averaged phase slope tends to identify gross shifts between the reference and each subsequent dynamic acquisition. Further, averaging permits the algorithm to be less sensitive to random phase fluctuations that it would be highly susceptible to, if we were to perform a local phase correction per point in k-space. However, there are other degrees of motion such as rotation, distortions and respiratory and cardiac motions, that are commonly encountered during the scan. The assumption of no intrakeyhole motion itself does not strictly hold and this combined with heart motion contributes to the low amplitude flutter that is seen on many subtraction images.

An established technique to adaptively correct for both intra and inter-view motion is the navigator echo (NAV) acquisition.[29] In this method, an additional echo ~~(NAV)~~ is acquired per phase encoding echo. Since the TR is short (~10 ms) for the 3D SPGR sequence used for this study, acquisition of the additional navigator echos would substantially increase the scan time, thereby reducing the dynamic temporal sampling rate. Alternatively, a single navigator echo can be acquired each, along $ky=0$ and $kz=0$, with $kx=0$ being acquired as part of the dynamic acquisition. This would add negligible time to the 3D acquisition, main-

taining the desired high temporal sampling rate. In effect, this approach makes the assumption that a single set of displacements in x, y, and z can summarize the motion artifact over the entire volume acquisition. This is similar to the basic assumptions described in this paper. Furthermore, since a displacement in space corresponds to a linear phase roll in k-space, the phase estimation technique described in this paper is considered appropriate to detect and correct the expected motions. The averaging over multiple echoes in the dataset serves to provide some degree of noise insensitivity.

In summary, the motion correction algorithm presented in this paper successfully reduces gross translational motion by estimating an averaged linear phase deviation per spatial frequency axis, between the reference and dynamic datasets. Where motion was negligible or could be attributed to other sources, implementation of the algorithm was not detrimental to the original data. If the nature of motion was within the parameters of the model, fairly good correction in terms of improved visualization of structures of interest, reduction in subtraction edges, and suppression of background ghost artifact and blurring was observed.

[a]Author to whom correspondence should be addressed. Telephone: (734)-936-8866; Fax: (734)-764-2412.

[1]S. H. Heywang, R. Bassermann, G. Fenzl *et al.*, "MRI of the breast: histopathological correlation," Eur. J. Radiol. **7**, 175–182 (1987).

[2]S. H. Heywang, D. Hahn, H. Schmidt *et al.*, "MR imaging of the breast using gadolinium-DTPA," J. Comput. Assist. Tomogr. **10**, 199–204 (1986).

[3]S. E. Harms, D. P. Flamig, K. I. Hesley *et al.*, "Mr imaging of the breast with rotating delivery of excitation off resonance: clinical experience with pathologic correlation," Radiology **187**, 493–501 (1993).

[4]S. G. Orel, M. D. Schnall, C. M. Powell *et al.*, "Staging of suspected breast cancer: effect of MR imaging and MR-guided biopsy," Radiology **196**, 115–22 (1995).

[5]W. A. Kaiser and E. Zeitler, "MR imaging of the breast: fast imaging sequences with and without Gd-DTPA," Radiology **170**, 681–686 (1989).

[6]M. D. Schnall, S. Orel, and L. Muenz, "Analysis of time intensity curved for enhancing breast lesions (abstr)," in *Proceedings of the Society of magnetic Resonance in medicine* (Berkeley, California Society of Magnetic Resonance in Medicine, 1993), p. 120.

[7]J. P. Stack, O. M. Redmond, M. B. Codd, P. A. Derva, and J. T. Ennis, "Breast disease: tissue characterization with Gd-DTPA enhancement profiles," Radiology **174**, 491–494 (1990).

[8]F. W. Flickinger, J. D. Allison, R. M. Sherry, and J. C. Wright, "Differentiation of benign from malignant breast masses by time-intensity evaluation of contrast enhanced MRI," Magn. Reson. Imaging **11**, 617–620 (1993).

[9]N. Seidner, J. P. Semple, W. R. Welch, and J. Folkman, "Tumor angiogenesis and metastasis: correlation in invasive breast carcinoma," N. Engl. J. Med. **324**, 1–8 (1991).

[10]J. Folkman, "What is the evidence that tumors are angiogensis dependent?," J. Natl. Cancer Inst. **82**, 4–6 (1990).

[11]A. L. Harris and E. Horak, "Growth factors and angiogenesis in breast cancer. Recent results," Cancer Res. **127**, 35–41 (1993).

[12]H. M. Jensen, J. Chen, M. R. DeVault, and A. E. Lewis, "Angiogenesis induced by "normal" human breast tissue: a probable marker for precancer," Science **218**, 293–295 (1982).

[13]S. H. Heywang-Korbrunner, "Contrast-enhanced magnetic resonance imaging of the breast," Invest. Radiol. **29**, 94–104 (1994).

[14]T. A. Spraggins, E. S. de Paredes, G. A. De Angelis, and F. Thiele, "Three dimensional keyhole imaging: application of dynamic contrast enhanced MRI of breast lesions (abstr)," in *Proceedings of the Society of Magnetic Resonance Imaging in Medicine* (Berkeley, California Society of Magnetic Resonance in Medicine, 1993), p. 118.

[15]S. E. Harms, D. P. Flamig, and K. L. Hesley, "Fat-suppressed three-dimensional MR imaging of the breast," RadioGraphics **13**, 247–267 (1993).

[16]Z. P. Liang and P. C. Lauterbur, "An efficient method for dynamic magnetic resonance imaging," IEEE Trans. Med. Imaging **10**(4), 677–686 (1994).

[17]V. Rasche, R. Proksa *et al.*, "Helical scan for time resolved MRI at 0.5*T* (abstr)," in *Proceeding of the Society of Magnetic Resonance in Medicine* (Berkeley, California, Society of Magnetic Resonance in Medicine, 1993), p. 479.

[18]J. W. Black, D. M. Ikeda, R. J. Herfkens *et al.*, "Magnetic Resonance Imaging of Breast Disease Using a Dynamic Spiral Sequence," in *Proceedings of the International Society of Magnetic Resonance in Medicine* (Berkeley, California, Society of Magnetic Resonance in Medicine, 1996), p. 749.

[19]J. J. Van Vaals, M. E. Brummer, W. T. Dixon *et al.*, "Keyhole method of accelerating imaging of contrast agent uptake," Magn. Reson. Imaging **3**, 671–675 (1993).

[20]D. B. Plewes and J. Bishop *et al.*, "Errors in quantitative dynamic three-dimensional keyhole MR imaging of the breast," Magn. Reson. Imaging **5**(3), 361–4 (1995).

[21]T. L. Chenevert and J. G. Pipe "Dynamic 3D imaging at high temporal resolution via reduced k-space sampling (abstr)," in *Proceeding of the Society of Magnetic Resonance in Medicine* (Berkeley, California, Society of Magnetic Resonance in Medicine, 1993), p. 1262.

[22]T. L. Chenevert, M. A. Helvie, A. M. Aisen, I. R. Francis *et al.*, "Dynamic three-dimensional imaging with partial K-space sampling: Initial application for Gadolinium enhanced rate characterization of breast lesions," Radiology **196**(1), 135–42 (1995).

[23]H. W. Korin, F. Farzaneh, R. C. Wright, and S. J. Riederer, "Compensation for the effects of linear motion in MR imaging," Magn. Reson. Med. **129**(1), 99–113 (1989).

[24]V. J. Wedeen, R. E. Wendt, and M. Jerosch-Herold, "Motion phase artifacts in Fourier transform MRI," Magn. Reson. Med. **11**(1), 114–120 (1989).

[25]E. M. Haacke and J. L. Patric, "Reducing motion artifacts in two-dimensional Fourier Transform imaging," Magn. Reson. Med. **4**, 359–376 (1986).

[26]M. Hedley and H. Yan, "Motion artifact suppression: A review of post-processing techniques," Magn. Reson. Imaging **10**, 627–635 (1992).

[27]M. Hedley, H. Yan, and D. Rosenfeld "Motion artifact correction in MRI using generalized projections," IEEE Trans. Med. Imaging **10**, 40–46 (1991).

[28]R. N. Bracewell, *The Fourier Transform and its Applications* (McGraw-Hill, New York, 1986), pp. 104–105.

[29]J. P. Felmlee, R. L. Ehman, D. I. Riederer, and H. W. Korin, "Adaptive Motion Compensation in MRI: Accuracy of motion measurements," Magn. Reson. Med. **18**, 207–213 (1991).